Article

Cell Metabolism

Sensing and Transmitting Intracellular Amino Acid Signals through Reversible Lysine Aminoacylations

Graphical Abstract

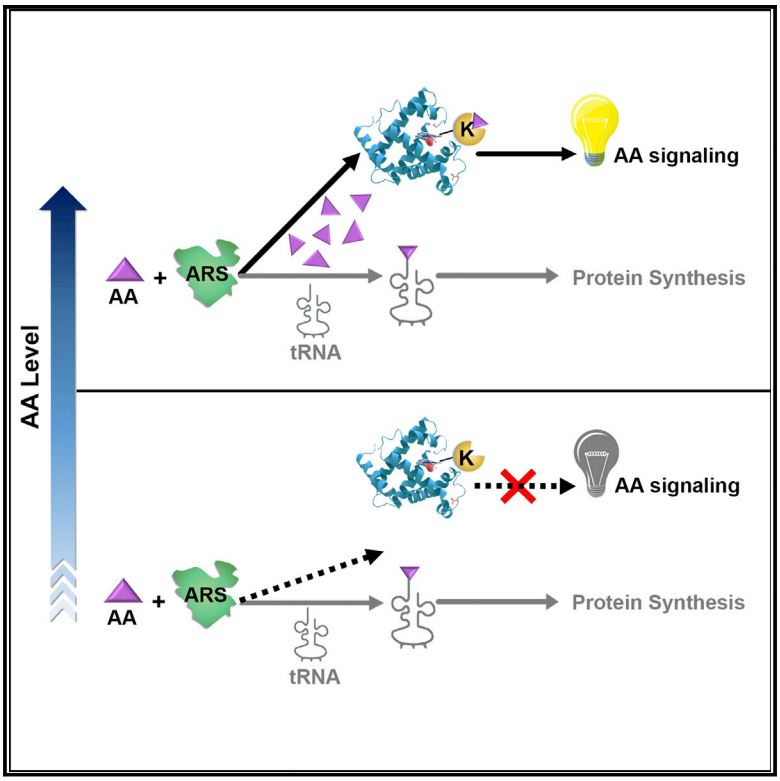

Authors

Xia-Di He, Wei Gong, Jia-Nong Zhang, ..., Yanhui Xu, Wei Xu, Shi-Min Zhao

Correspondence

xuyh@fudan.edu.cn (Y.X.), xuwei_0706@fudan.edu.cn (W.X.), zhaosm@fudan.edu.cn (S.-M.Z.)

In Brief

He et al. reveal that tRNA synthetases sense sufficiency of amino acids and act as aminoacyl transferases to modify ε-amines of lysines in proteins, with leucylation of RagA/B regulating mTORC1 activity and glutaminylation of ASK1 inhibiting apoptosis. Lysine aminoacylation marks are removed by SIRT1 and SIRT3.

Highlights

- Amino acids modify ε-amines of lysines
- Each tRNA synthetase is the aminoacyl transferase of its cognate amino acid
- Aminoacylations can be reversed by deacetylases
- Aminoacylations transmit amino acid signals to regulate cellular functions

He et al., 2018, Cell Metabolism *27*, 1–16
January 9, 2018
https://doi.org/10.1016/j.cmet.2017.10.015

CellPress

Please cite this article in press as: He et al., Sensing and Transmitting Intracellular Amino Acid Signals through Reversible Lysine Aminoacylations, Cell Metabolism (2017), https://doi.org/10.1016/j.cmet.2017.10.015

Cell Metabolism
Article

Sensing and Transmitting Intracellular Amino Acid Signals through Reversible Lysine Aminoacylations

Xia-Di He,[1,2,5] Wei Gong,[1,3] Jia-Nong Zhang,[1,2,5] Ji Nie,[1,2,5] Cui-Fang Yao,[1,2,5] Fu-Shen Guo,[1,2] Yan Lin,[1,2] Xiao-Hui Wu,[1,4] Feng Li,[1,2,5] Jie Li,[1,3] Wei-Cheng Sun,[6] En-Duo Wang,[6] Yan-Peng An,[1,2] Hui-Ru Tang,[1,2] Guo-Quan Yan,[1] Peng-Yuan Yang,[1] Yun Wei,[1,2] Yun-Zi Mao,[1,2] Peng-Cheng Lin,[8] Jian-Yuan Zhao,[1,5] Yanhui Xu,[1,3,7,*] Wei Xu,[1,2,*] and Shi-Min Zhao[1,2,5,9,*]

[1]Obstetrics and Gynecology Hospital of Fudan University, State Key Lab of Genetic Engineering, School of Life Sciences and Institutes of Biomedical Sciences

[2]Key Laboratory of Reproduction Regulation of NPFPC (SIPPR,IRD) and Collaborative Innovation Center for Genetics and Development

[3]Fudan University Shanghai Cancer Center

[4]Institute of Developmental Biology and Molecular Medicine
Fudan University, Shanghai 200032, PRC

[5]State Key Laboratory of Biotherapy/ Collaborative Innovation Center for Biotherapy, West China Hospital, Sichuan University, Chengdu 610041, PRC

[6]Institute of Biochemistry and Cell Biology, Shanghai Institutes for Biological Sciences

[7]CAS Center for Excellence in Molecular Cell Science
Chinese Academy of Sciences, Shanghai 200031, PRC

[8]Key Laboratory for Tibet Plateau Phytochemistry of Qinghai Province, College of Pharmacy, Qinghai University for Nationalities, Xining 810007, PRC

[9]Lead Contact

*Correspondence: xuyh@fudan.edu.cn (Y.X.), xuwei_0706@fudan.edu.cn (W.X.), zhaosm@fudan.edu.cn (S.-M.Z.)

https://doi.org/10.1016/j.cmet.2017.10.015

SUMMARY

Amino acids are known regulators of cellular signaling and physiology, but how they are sensed intracellularly is not fully understood. Herein, we report that each aminoacyl-tRNA synthetase (ARS) senses its cognate amino acid sufficiency through catalyzing the formation of lysine aminoacylation (K-AA) on its specific substrate proteins. At physiologic levels, amino acids promote ARSs bound to their substrates and form K-AAs on the ε-amine of lysines in their substrates by producing reactive aminoacyl adenylates. The K-AA marks can be removed by deacetylases, such as SIRT1 and SIRT3, employing the same mechanism as that involved in deacetylation. These dynamically regulated K-AAs transduce signals of their respective amino acids. Reversible leucylation on ras-related GTP-binding protein A/B regulates activity of the mammalian target of rapamycin complex 1. Glutaminylation on apoptosis signal-regulating kinase 1 suppresses apoptosis. We discovered non-canonical functions of ARSs and revealed systematic and functional amino acid sensing and signal transduction networks.

INTRODUCTION

The three major nutrients utilized by cells are glucose, fatty acids, and amino acids, and are sensed through distinct mechanisms. The intake, storage, mobilization, and breakdown of glucose and fatty acids are mediated by various sensors (Chantranupong et al., 2015; Efeyan et al., 2015). For example, the extracellular glucose levels and their cross-plasma membrane transportation are sensed and mediated by the glucose transporters (Thorens and Mueckler, 2010), while the fatty acids are sensed by acyl-coenzyme A (CoA)-binding proteins that monitor the intracellular trafficking and utilization of long-chain fatty acids (Faergeman et al., 2007). As for amino acids, the general control non-derepressible 2 (GCN2) protein indirectly senses the abundance of intracellular amino acids by binding tightly to uncharged tRNA molecules and preventing the initiation of translation by inactivating eukaryotic translation initiation factor 2α (Berlanga et al., 1999; Dong et al., 2000). The mammalian target of rapamycin complex 1 (mTORC1) is known to respond to several amino acids in the lysosome membrane (Zoncu et al., 2011). Amino acid transporters are also proposed to be extracellular amino acid sensors (Rebsamen et al., 2015; Taylor, 2014; Wang et al., 2015). However, the chemical bases of these proposed amino acid sensing and transmitting molecules are yet to be defined. Sestrin2 and CASTOR1, GATOR2-interacting proteins, which bind leucine and arginine, respectively, at physiological concentrations and activate mTORC1 by disrupting the Sestrin2- or CASTOR1-GATOR2 interactions (Chantranupong et al., 2016; Wolfson et al., 2016), represent the very few reported amino acid sensors whose sensing and transmitting mechanisms are adequately defined. Significant data gaps exist with respect to understanding whether systematic amino acid sensing and regulating mechanisms exist, given the numerous known regulatory functions of amino acids.

To be considered as a bona fide amino acid sensor, the protein must directly and specifically bind to an amino acid. Aminoacyl-tRNA synthetases (ARSs) are a family of enzymes capable of binding and discriminating among amino acids and catalyzing

Metabolites Released from Human Liver Cancer Proteome by CobB or SIRT3														
Amino Acids					Other Metabolites									
No.	Metabolites	Structure	Cleaved by		No.	Metabolites	Structure	Cleaved by		No.	Metabolites	Structure	Cleaved by	
			CobB	SIRT3				CobB	SIRT3				CobB	SIRT3
1	Glycine		√	√	21	Propanoic acid		√	√	41	2-phenylbutyric acid	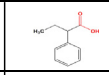	√	X
2	Alanine		√	√	22	Pyruvate		√	√	42	Heptanedioic acid,1-methyl ester	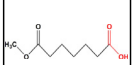	√	√
3	Serine		√	√	23	Lactate		√	√	43	Cystathionine	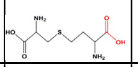	√	X
4	Proline		√	√	24	1-aminocyclopropane carboxylic acid		√	X	44	Hexadecanoic acid		√	√
5	Valine		√	√	25	Pentanoic acid		√	√	45	cis-6-octadecenoic acid	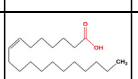	√	√
6	Threonine		√	√	26	Glyceric acid		√	√	46	Arachidonic acid	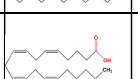	√	X
7	Cysteine		√	√	27	Fumarate		√	X	47	5,8,11-eicosatriynoic acid	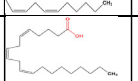	√	√
8	Leucine		√	√	28	Maleate		√	X	48	Prostaglandin F2a	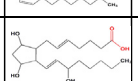	√	X
9	Isoleucine		√	√	29	3-methyl-2-ketobutyric acid		√	√	49	Prostaglandin E1	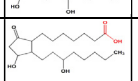	√	√
10	Asparagine		√	√	30	Methylmalonic acid monoamide		√	√					
11	Aspartate		√	√	31	Succinate		√	X					
12	Glutamine		√	√	32	2-piperidinecarboxylic acid		√	√					
13	Lysine		√	√	33	2-hydroxyhexanoic acid		√	√					
14	Glutamate		√	√	34	Iminodiacetic acid		√	X					
15	Methionine		√	√	35	2-Thiazolidinecarboxylic acid		√	√					
16	Histidine		√	√	36	Malate		√	X					
17	Phenylalanir		√	√	37	Dimethylsulphonioprop ionate		√	√					
18	Arginine		√	√	38	α-ketoglutarate		√	X					
19	Tyrosine		√	√	39	2,6-dihydroxy benzoic acid		√	√					
20	Tryptophan		√	√	40	N-Isovalerylglycine		√	X					

Figure 1. Aminoacylations Present and Regulated in Cells

The names and structures of CobB- or SIRT3-released metabolites from the liver cancer proteome (n = 3) are presented. Metabolites that were released by either CobB or SIRT3 are marked by "√" and metabolites that were not released by them are marked by "X." The carboxyl groups in all structures are marked in red. See also Figure S1.

A

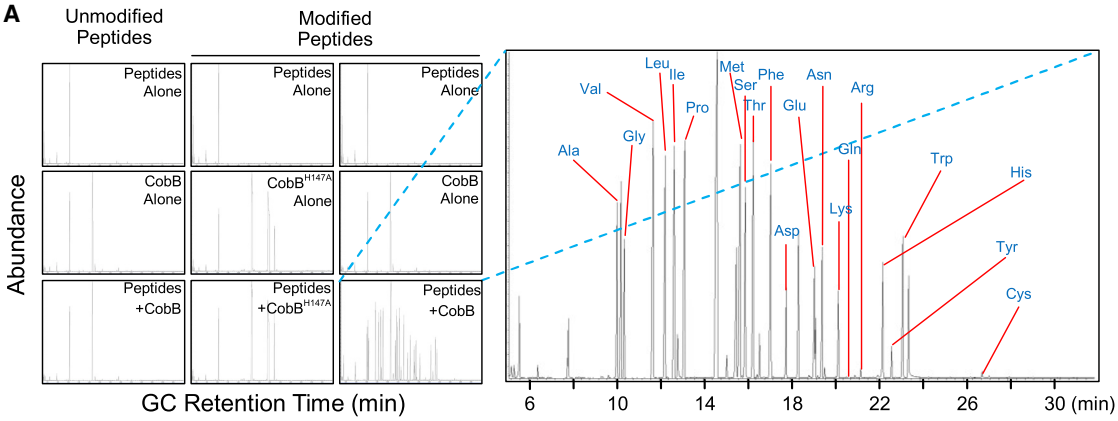

B

Relative levels of Amino Acids Released from Proteome of HEK293T Cells by CobB						
Fractions	Cytosol		Mitochondria		Nuclear	
NAD^+	+	−	+	−	+	−
Ala	273.4 ± 26.1	1.3 ± 0.4	187.1 ± 8.1	1.1 ± 0.3	310.1 ± 25.3	0.8 ± 0.4
Arg	118.3 ± 14.3	1.5± 0.7	250.3 ± 12.5	1.2 ± 04	94.2 ± 4.7	1.2 ± 0.3
Asn	204.5 ± 17.6	1.0 ± 0.2	136.6 ± 7.8	0.9 ± 0.2	187.4 ± 7.9	1.1 ± 0.2
Asp	169.3 ±9.6	1.3 ± 0.7	179.8 ± 5.9	1.4 ± 0.5	124.6 ± 8.2	0.9 ± 0.3
Cys	117.6 ± 14.8	1.4 ± 0.5	243.2 ± 14.4	1.2 ± 0.6	213.7 ± 13.8	1.5 ± 0.4
Gln	234.5 ± 15.3	1.0 ± 0.4	152.0 ± 12.4	0.8 ± 0.2	114.2 ± 6.2	1.2 ± 0.2
Glu	96.4 ± 7.8	1.1 ± 0.3	205.4 ± 21.7	1.3 ± 0.5	124.6 ± 9.1	0.8 ± 0.3
Gly	194.9 ± 13.1	1.7 ± 0.8	64.3 ± 7.5	1.0 ± 0.3	178.3 ± 10.7	1.1 ± 0.3
His	76.2 ±6.3	0.8 ± 0.4	203.5 ± 9.2	1.4 ± 0.6	88.3 ± 4.3	0.9 ± 0.2
Ile	250.7 ± 28.2	1.0 ± 0.6	263.1 ± 10.7	1.1 ± 0.4	241.2 ± 17.5	1.0 ± 0.1
Leu	346.1 ± 17.6	1.1 ± 0.5	221.0 ± 13.5	1.0 ± 0.2	290.1 ± 14.4	1.3 ± 0.4
Lys	156.5 ± 8.2	1.3 ± 0.4	84.2 ± 7.6	1.5 ± 0.7	74.3 ± 5.6	1.7 ± 0.7
Met	184.1 ± 9.8	1.2 ± 0.5	125.9 ± 9.1	1.3 ± 0.6	169.4 ± 15.8	1.0 ± 0.3
Phe	361.0 ± 16.1	0.9 ± 0.3	189.2 ± 16.3	0.9 ± 0.4	239.1 ± 11.2	1.0 ± 0.2
Pro	225.0 ± 11.6	1.3 ± 0.4	133.0 ± 8.8	1.1 ± 0.3	240.6 ± 16.3	1.1 ± 0.3
Ser	44.5 ± 3.8	0.8 ± 0.4	85.1 ± 7.1	0.9 ± 0.2	65.2 ± 7.3	1.0 ± 0.2
Thr	197.9 ± 10.2	1.4 ± 0.5	125.6 ± 7.2	1.2 ± 0.4	106.7 ± 8.1	1.4 ± 0.5
Trp	221.3 ± 13.5	1.3 ± 0.6	132.4 ± 9.3	1.4 ± 0.6	271.2 ± 13.6	1.2 ± 0.4
Tyr	215.6 ± 17.1	1.0 ± 0.2	267.1 ± 12.5	1.1 ± 0.3	214.7 ±18.1	0.8 ± 0.2
Val	243.1 ± 20.9	1.2 ± 0.4	261.9 ± 17.6	1.4 ± 0.8	128.4 ± 9.5	1.5 ± 0.4

C

Number of K-AAs Identified from Proteome of Liver Cancer Tissue			
K-AAs	No. of Proteins	No. of Peptides	No. of Sites
A	239	252	389
R	146	148	201
N	235	250	351
D	229	242	363
C	249	252	414
Q	118	120	196
E	199	205	316
G	267	286	414
H	158	161	239
L/I	268	274	373
K	110	112	165
M	199	202	330
F	136	136	258
P	184	186	275
S	172	176	338
T	169	173	288
W	140	143	199
Y	154	159	228
V	202	207	332

D

Sites	Leucylation (%)	
	Leu(0.05mM)	Leu（0.4mM）
$RagA^{K142}$/ $RagB^{K203}$	10.5±1.9	35.6±8.7

E

Sites	Glutaminylation (%)	
	Gln (1mM)	Gln (8mM)
$ASK1^{K688}$	12.5±2.2	27.6±10.2

Figure 2. Substantial K-AAs Are Widespread in Cells

(A) The synthetic lysine modified peptides listed in Figures S1F and S1G and their corresponding unmodified peptides were each mixed and treated with recombinant CobB. The modified peptide library was also treated with $CobB^{H147A}$. The released amino acids were derivatized and analyzed by GC followed by MS. GC peaks corresponding to each amino acid (confirmed by MS/MS) were marked. See also Figures S1F and S1G.

(legend continued on next page)

aminoacylation reactions to link each specific amino acid to its cognate tRNA, and thus fulfill this requirement as true amino acid sensors. Remarkably, some ARSs and their corresponding amino acids regulate the same functions other than protein synthesis. For example, both leucine and leucyl-tRNA synthetase (LARS) activate mTORC1 (Blomstrand et al., 2006; Han et al., 2012; Yoon et al., 2016). Glutamine and glutamine-bound glutaminyl-tRNA synthetase (QARS) both suppress apoptosis by inhibiting the pro-apoptotic enzyme apoptosis signal-regulating kinase 1 (ASK1) (Hattori et al., 2009; Ko et al., 2001). Moreover, the binding of amino acids to their corresponding ARSs is required for signal transmission by the latter (Guo and Schimmel, 2013; Han et al., 2012; Ko et al., 2001). These facts support the concept that amino acids are sensed by ARSs.

Metabolite-derived, amide-bonded post-translational modifications (PTMs) are regulated by the levels of respective metabolites, raising the possibility that these PTMs sense metabolites. Lysine (Gilreath et al., 2011; Yanagisawa et al., 2010) and methionine (Hountondji et al., 2000) are also among the amide-bonded modifiers of lysine. Notably, these two lysine aminoacylations are catalyzed by their corresponding ARSs, suggesting again the possibility that ARSs, which are capable of producing reactive aminoacyl-adenylates (aminoacyl-AMPs), high-energy aminoacyl-phosphate bonds containing compounds that are known to modify the ε-amine groups of lysines (Moellering and Cravatt, 2013; Weinert et al., 2013), may catalyze lysine aminoacylation (K-AA) formation.

RESULTS

Identification of Lysine Aminoacylations in Cells

We employed recombinant *Salmonella* deacetylase CobB (Figure S1A), a documented multi-specific amidase (Colak et al., 2013), to cleave lysine modifications that are present in the human liver cancer proteome, in which the non-covalently bonded metabolites were removed through repeated washing with 90% acetone before CobB treatments (Figure S1B). As oximation treatment of CobB cleaved modifiers, assumed to be *O*-acyl-ADP-ribose (Blander and Guarente, 2004), by methoxyamine hydrochloride resulted in free acids (Figures S1C and S1D), the modifiers were directly annotated by their derivatized *m/z* values following mass spectrometry (MS) analysis.

Positively identified metabolites, which had an at least 2-fold increase in abundance in CobB-treated relative to that of untreated proteome, were validated by comparing both the retention time of gas chromatography (GC) and spectra of MS with those of standard metabolites (Figure S1E). In experiments conducted in triplicate, 49 metabolites, including known amide-bonded modifiers of lysine such as propionic acid, succinate, pentanoic acid, and hexadecanoic acid (Chen et al., 2007; Kato, 2014; Zhang et al., 2011), were positively identified (Figure 1).

K-AAs Are Widespread in Cells and Respond to Amino Acid Levels

All 20 amino acids were released from the liver cancer proteome by CobB (Figure 1). To validate that amino acids are potential lysine modifiers, we synthesized peptide libraries that were either devoid of or contained all 20 standard amino acids amide bonded to ε-amine of lysines in the peptides (Figures S1F and S2A) and tested the ability of CobB to cleave these lysine aminoacylations from these peptides. CobB lacks peptidase activity, since it failed to release any amino acid from the unmodified peptide library (Figure 2A). Moreover, wild-type CobB, but not inactivated CobB^{H147A} (Holden et al., 2004), cleaved amino acids from the modified peptides (Figure 2A). Furthermore, CobB released all 20 standard amino acids from the metabolite-free proteome of isolated nuclear, cytosolic, and mitochondrial fractions of HEK293T cells in an NAD^+-dependent manner (Figure 2B). These results confirmed that CobB released K-AAs from liver cancer proteome. Lastly, in three independent experiments, searching for K-AAs in a tryptic peptide library of human liver cancer identified large numbers of proteins, whose functions covered almost all aspects of cell physiology, as substrates of K-AAs (Figure 2C; Table S1), and confirmed that K-AAs are widespread in human cells.

We quantified K-AA levels on identified leucylated and glutaminylated lysines (Table S1) and found that increasing leucine increased cellular leucylation levels of lysine 142 (K142) of Ras-related guanosine triphosphate (GTP)-binding protein A (RagA) or lysine 203 (K203) of Ras-related GTP-binding protein B (RagB), given they share the same sequence, from 10.5% to 35.6% in HEK293T cells (Figure 2D), and that increasing glutamine elevated the glutaminylation level of lysine 688 (K688) of apoptosis signal-regulating kinase 1 (ASK1) (Table S1) from around 12.5% to 27.6% in HEK293T cells (Figure 2E). These results confirmed that K-AAs are dynamically regulated by amino acid levels.

ARSs Are Aminoacyl Transferases

ARSs catalyze the formation of reactive aminoacyl-phosphate bond-containing aminoacyl-AMPs, which may form K-AAs (Figure 3A). LARS resulted in an adduct, which produced the same tandem MS (MS/MS) spectrum of a synthetic K142 leucylated-containing RagA peptide, between synthetic K142 RagA in an amino acid-, ATP-, and ARS-dependent manner (Figure 3B). All purified cytoplasmic ARSs were found to add molecular weights equal to their respective aminoacylations to the synthetic N terminus-protected, substrate-derived peptides (Figures S1F, S1G, and S2A). Moreover, all 17 isolated functional mitochondrial ARS2s also added molecular weights identical to K-AAs in their corresponding synthetic mitochondrial substrate-derived peptides (Figure S2B), except that the formation of arginylation, glutaminylation, and glutamylation required the presence of their corresponding tRNAs to activate their

(B) Changes in the relative amino acid levels (folds, normalized to the untreated proteome) because of CobB treatment (n = 3, mean ± SD) of the proteome of the cytosolic, nuclear, and mitochondrial fractions of HEK293T cells are shown.

(C) Numbers of proteins, peptides, and sites for each K-AA identified in the human liver cancer proteome are summarized. K_{Leu} and K_{Ile} were summarized together since they were indistinguishable in the survey.

(D) Levels of leucylation of K142 of RagA and/or K203 of RagB were determined (n = 3, mean ± SD) upon leucine supplementation (0.4 mM).

(E) Levels of glutaminylation of K688 of ASK1 were determined (n = 3, mean ± SD) under low (1 mM) and high (8 mM) glutamine.

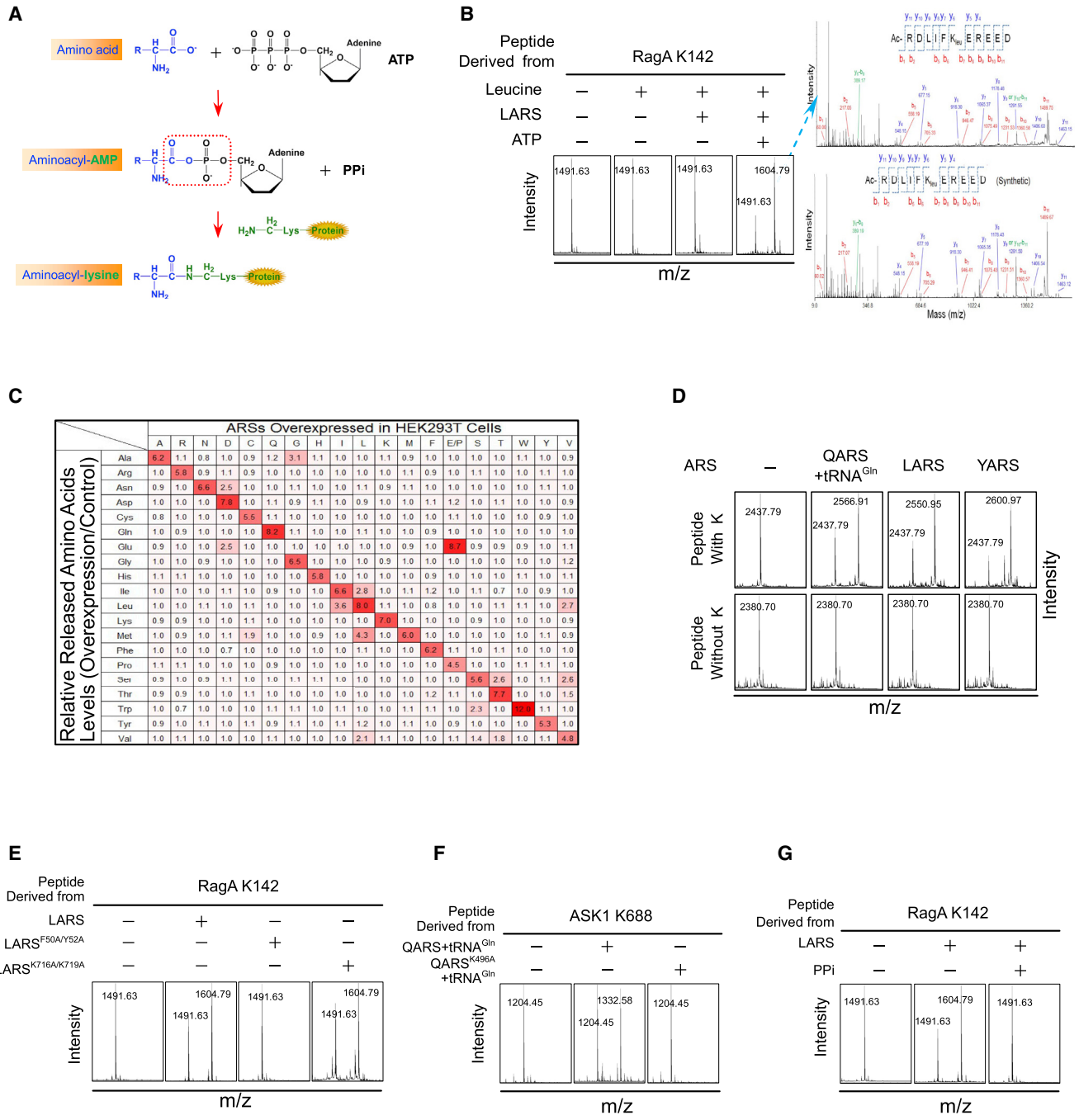

	A	R	N	D	C	Q	G	H	I	L	K	M	F	E/P	S	T	W	Y	V
Ala	6.2	1.1	0.8	1.0	0.9	1.2	3.1	1.1	1.0	1.0	1.1	0.9	1.0	1.0	1.0	1.0	1.1	1.0	0.9
Arg	1.0	5.8	0.9	1.1	0.9	1.0	1.0	1.0	1.0	1.0	1.0	1.1	0.9	1.0	1.1	1.0	1.0	1.1	1.0
Asn	0.9	1.0	6.6	2.5	1.0	1.0	1.1	1.0	1.0	1.1	0.9	1.1	1.0	1.0	1.0	1.0	1.0	1.1	1.0
Asp	1.0	1.0	1.0	7.8	1.0	1.1	0.9	1.1	1.0	0.9	1.0	1.0	1.1	1.2	1.0	1.1	1.0	1.0	0.9
Cys	0.8	1.0	1.0	1.0	5.5	1.1	1.0	1.0	1.0	1.0	1.0	1.0	1.0	1.1	1.0	1.0	1.0	0.9	1.0
Gln	1.0	0.9	1.0	1.0	1.0	8.2	1.1	1.0	1.0	1.1	1.0	1.0	0.9	1.0	1.0	1.0	1.0	1.0	1.0
Glu	0.9	1.0	1.0	2.5	1.0	1.0	1.0	1.0	1.0	1.0	1.0	0.9	1.0	8.7	0.9	0.9	0.9	1.0	1.1
Gly	1.0	1.0	0.9	1.0	1.0	1.0	6.5	1.0	1.0	1.0	0.9	1.0	1.0	1.0	1.0	1.0	1.0	1.0	1.2
His	1.1	1.1	1.0	1.0	1.0	1.0	1.0	5.8	1.0	1.0	1.0	1.0	0.9	1.0	1.0	1.0	1.1	1.0	1.1
Ile	1.0	1.0	1.0	1.1	1.0	0.9	1.0	1.0	6.6	2.8	1.0	1.1	1.2	1.0	1.1	0.7	1.0	0.9	1.0
Leu	1.0	1.0	1.1	1.0	1.1	1.0	1.0	1.0	3.6	8.0	1.1	1.0	0.8	1.0	1.0	1.1	1.1	1.0	2.7
Lys	0.9	0.9	1.0	1.0	1.1	1.0	1.0	1.0	1.0	1.0	7.0	1.0	1.0	1.0	0.9	1.0	1.0	1.0	0.9
Met	1.0	0.9	1.0	1.1	1.9	1.0	1.0	0.9	1.0	4.3	1.0	6.0	1.0	1.0	1.0	1.0	1.0	1.1	0.9
Phe	1.0	1.0	1.0	0.7	1.0	1.0	1.0	1.0	1.0	1.1	1.0	1.0	6.2	1.1	1.0	1.1	1.0	1.0	1.0
Pro	1.1	1.1	1.0	1.0	1.0	0.9	1.0	1.0	1.0	1.0	1.0	1.0	1.0	4.5	1.0	1.0	1.1	1.1	1.0
Ser	0.9	1.0	0.9	1.1	1.0	1.0	1.1	1.1	1.0	1.0	1.0	1.0	1.0	1.0	5.6	2.6	1.0	1.1	2.6
Thr	0.9	0.9	1.0	1.0	1.1	1.0	1.0	1.0	1.0	1.0	1.0	1.0	1.2	1.1	1.0	7.7	1.0	1.0	1.5
Trp	1.0	0.7	1.0	1.0	1.0	1.1	1.1	1.0	1.1	1.0	1.0	1.1	1.1	1.0	2.3	1.0	12.0	1.1	1.0
Tyr	0.9	1.0	1.1	1.0	1.1	0.9	1.1	1.0	1.1	1.2	1.0	1.1	1.0	0.9	1.0	1.0	1.0	5.3	1.0
Val	1.0	1.1	1.0	1.0	1.0	1.1	1.0	1.0	1.0	2.1	1.1	1.0	1.0	1.1	1.4	1.8	1.0	1.1	4.8

Figure 3. ARSs Catalyze K-AA Formation

(A) Proposed mechanisms for the ARS-catalyzed generation of K-AAs. Reactive carboxyl phosphate bond is circled.

(B) Representative results of ARSs catalyze K-AAs formation. Synthetic K142-containing RagA peptide (RagA K142) was leucylated by LARS *in vitro*. The formation of $K_{Leu}142$ was detected by MS (left). The MS/MS spectrum of the leucylated product (right upper) was compared with that of a synthetic leucylated K142 peptide (right lower). See also Figures S2A and S2B.

(C) ARSs were overexpressed in HEK293T cells. Amide-bonded amino acids in the proteome of the cytosolic fraction of ARS-expressing cells and control cells were cleaved by CobB, as analyzed by MS (n = 3, means). ARS-expressing/control ratios were indicated by intensities of red color. See also Figures S2C and S2D.

(D) Synthetic N-acetylated peptide containing all 20 proteogenic amino acids (Ac-HDRFACGQEKLMNSYTIWPV, upper) and the same peptide with lysine switched to alanine (lower) were each tested for their abilities to be modified by QRS, LARS, and YARS.

(E) Purified LARS, leucine-binding-deficient $LARS^{F50A/Y52A}$, and $tRNA^{Leu}$ charging-defective $LARS^{K716A/K719A}$ were tested for their abilities to catalyze K_{Leu} formation in the synthetic K142 peptide.

(legend continued on next page)

corresponding ARSs (Kern and Lapointe, 1981; Nazario and Evans, 1974; Ravel et al., 1965) (Figures S2A and S2B). Furthermore, in HEK293T cells the overexpression of ARSs and ARS2s (Figure S2C) resulted in increased levels of corresponding K-AAs in the cytosol (Figure 3C) and mitochondria (Figure S2D), respectively, whereas the knockdown of ARSs decreased the levels of the corresponding K-AAs in HEK293T cells (Figure S2E), confirming that ARSs are specific aminoacyl transferases functioning in cells. It is worth noting that few ARSs showed the ability to increase the K-AA levels of other amino acids (Figures 3C and S2D), consistent with previous reports that some ARSs also recognize other amino acids and may function as multi-specific aminoacyl transferases.

Notably, LARS, QARS, and tyrosyl-tRNA synthetase (YARS) only added corresponding amino acids on a synthetic peptide composed of all 20 standard amino acids, but not on the peptide with the same sequence but with lysine converted to alanine (Figure 3D), showing that ARSs catalyze modifications on lysine residues. Moreover, aminoacyl-AMP formation-defective LARS$^{F50A/Y52A}$ (Han et al., 2012) (Figure 3E), ATP-binding-defective QARS^{K496A} (Kodera et al., 2015) (Figure 3F), and inclusion of pyrophosphate to the reaction to inhibit leucyl-AMP production (Airas and Cramer, 1986) (Figure 3G) all failed to form K-AAs in synthetics peptides. However, tRNA charging-defective but leucyl-AMP-producing LARS$^{K716A/K719A}$ (Han et al., 2012) retained its ability to form leucylation (Figure 3E). These results collectively confirmed that ARSs exhibit their lysine aminoacyl transferase activity depending on their ability to produce aminoacyl-AMP.

Leucine and Glutamine Promote LARS-Substrate and QARS-Substrate Interactions and Substantial Substrate Aminoacylations

The K_M of leucine for LARS to leucylate RagA *in vitro* was 289.12 μM (Figure 4A) and the K_M of glutamine for QARS to glutaminylate ASK1 was 1,986.66 μM (Figure 4B); both were around the cellular levels of these two amino acids, showing that leucylation and glutaminylation are both capable of sensing intracellular leucine and glutamine, respectively. Moreover, both K142 of RagA and K688 of ASK1 were aminoacylated rapidly when leucine and glutamine, respectively, were at high levels (Figures 4A and 4B), showing that K-AAs are efficient amino acid level readouts. Furthermore, LARS, but not LARS$^{F50A/Y52A}$, increased leucylation levels on K142 of RagA from 8.5% to 51.3% and K307 of RagA from 4.2% to 14.1% in a leucine-dependent manner (Figure 4C). QARS, but not QARS^{K496A}, glutamine-dependently increased glutaminylation levels on lysines 657, 688, and 878 of ASK1 from 3.1% to 8.3%, from 11.0% to 43.4%, and from 2.2% to 6.8%, respectively (Figure 4D). These results showed that K-AAs modify a substantial percentage of specific lysines in their substrates and may regulate the properties of their substrates.

Importantly, we found that the presence of ARS protein in the aminoacylation reactions was required for aminoacylation reactions. A solution pre-incubated with leucine, LARS, and ATP to generate leucyl-AMP followed by removal of LARS with centrifugal filter leucylated neither intact RagA (Figure 4E), probing by a homemade K142 site-specific leucylation antibody (Figure S3A), nor K142 peptide of RagA (Figure 4G). Moreover, the presence of QARS in the reaction mix was also required for QARS to glutaminylate either K688 in intact ASK1 protein (Figure 4F), detected by a homemade K688 glutaminyl-lysine antibody (Figure S3B), or K688 peptide of ASK1 (Figure 4G). These results showed that ARS-produced aminoacyl-AMPs, unlike that of acetyl-phosphate, diffuse into solution and modify lysines non-specifically (Weinert et al., 2013), and selectively modify substrate proteins that physically interact with ARSs. Confirming this notion, the presence of GTP-bound RagD^{Q121L} in the reaction mix to increase LARS-RagA interaction caused higher leucylation of RagA^{K142} than those of wild-type RagD and guanosine diphosphate (GDP)-bound RagD^{S77L}, with both having weaker ability to bind LARS (Han et al., 2012), whereas the presence of LARS non-interacting RagC did not affect leucylation of RagA^{K142} (Figure S3C). Moreover, simultaneous overexpression of LARS and RagA in HEK293T cells increased the leucylation level of RagA via probing by a homemade pan-leucylation antibody (LeuK) (Figures S3D and S3E); however, switching N969 and K970 of LARS to alanine (LARS$^{N969A/K970A}$) to disrupt the LARS-Rag GTPase interaction (Han et al., 2012) impaired the ability of LARS to leucylate RagA (Figure 4H). Moreover, at around 0.4 mM, the leucine level that activates mTORC1 cells (Yoshida et al., 2015), leucine induces half-maximum LARS-RagA interaction and half-maximum K142 leucylation in RagA (Figure 4I). Similarly, at around 2 mM, the glutamine level that suppresses apoptosis in cells (Ko et al., 2001), glutamine induces half-maximum QARS-ASK1 interaction and half-maximum K688 glutaminylation in ASK1 (Figure 4J). These findings are consistent with previous reports that leucine enhances LARS-GTPase interaction (Han et al., 2012) and glutamine enhances QARS-ASK1 interaction both in cells and *in vitro* (Ko et al., 2001), and provides mechanistic explanations for how these amino acids are sensed by ARSs.

K-AAs Are Removed by Deacetylases

To identify possible human deaminoacylases, we screened deaminoacylase activities of NAD^+-dependent sirtuins, namely SIRT1–SIRT7 (Balakin et al., 2007; Du et al., 2011), in synthetic aminoacylated peptides (Figures S1F and S1G). Among them, SIRT1 was found to have deaminoacylase activity for eight types of K-AAs in synthetic peptides, including RagA K142 leucylation, but not K688 glutaminylation (Figures 5A and S2F). SIRT3, which functions in both the cytosol as a 399-amino-acid deacetylase (44 kDa, long form) and the mitochondria as a 257-amino-acid deacetylase (amino acids 143–399, 28 kDa, short form) (Law et al., 2009), showed deaminoacylase activity toward all synthetic K-AAs tested (Figures 5B and S2F). The deaminoacylase activity of SIRT3 extended to K-AAs in liver cancer proteome (Figure 1) and purified intact proteins from HEK293T cells.

(F) Purified QARS and ATP-binding-deficient QARS^{K496A} were tested for their ability to catalyze K-Gln formation in the synthetic ASK1-derived K688-containing peptide (K688 peptide). The tRNA^{Gln} was included in the reaction mix to activate the reaction.
(G) The formation of K_{Leu}142 in the synthetic K142 peptide, catalyzed by LARS, was tested in the absence and presence of inorganic pyrophosphate (PPi, 10 mM final concentration).

A

Kinetics of LARS			
Substrates	K_{cat}(s^{-1})	K_m(μM)	K_{cat}/K_m ($s^{-1}M^{-1}$)
Leucine (RagA Fixed at 0.05 mM)	2.36 ±0.17	289.12 ±36.95	8.16E3 ±2.98E2
RagAK142 (Leucine Fixed at 1 mM)	2.33 ±0.21	0.16 ±0.04	1.47E7 ±5.30E5

B

Kinetics of QARS			
Substrates	K_{cat}(s^{-1})	K_m(μM)	K_{cat}/K_m ($s^{-1}M^{-1}$)
Glutamine (ASK1 Fixed at 0.1 mM)	3.61 ±0.42	1986.66 ±151.13	1.82E3 ±8.36E1
ASK1K688 (glutamine Fixed at 10 mM)	3.63 ±0.55	0.29 ±0.02	1.26E7 ±2.36E5

C

Leucylated Sites	Leucylation Levels of RagA (%)					
	No LARS		LARS		$LARS^{F50A/Y52A}$	
	-Leu	+Leu	-Leu	+Leu	-Leu	+Leu
K142	8.0 ± 1.2	8.8 ± 2.4	8.5 ±1.7	51.3 ±6.4	9.7 ±1.8	10.2 ±2.2
K307	3.6 ± 1.4	3.3 ±0.6	4.2 ±1.5	14.1 ±4.5	3.5 ±1.2	3.1 ±0.9

D

Glutaminylated Sites	Glutaminylation Levels of ASK1 (%)					
	No QARS		QARS		$QARS^{K496A}$	
	-Gln	+Gln	-Gln	+Gln	-Gln	+Gln
K657	2.3 ± 1.1	2.8 ± 1.5	3.1 ±1.5	8.3 ±2.6	3.1 ±0.8	3.5 ±1.6
K688	8.6 ± 2.4	9.0 ± 2.2	11.0 ±3.5	43.4 ±8.3	10.4 ±3.3	10.8 ±4.6
K878	1.8 ± 0.5	2.1 ± 1.1	2.2 ±0.7	6.8 ±1.9	2.2 ±0.6	2.5 ±1.0

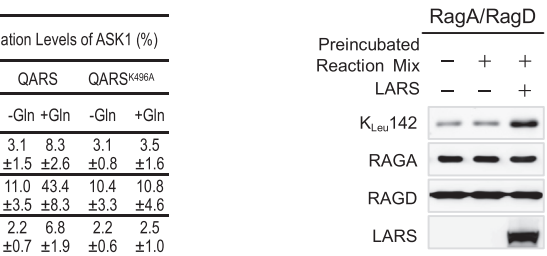

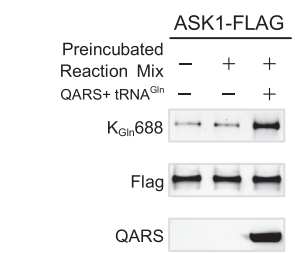

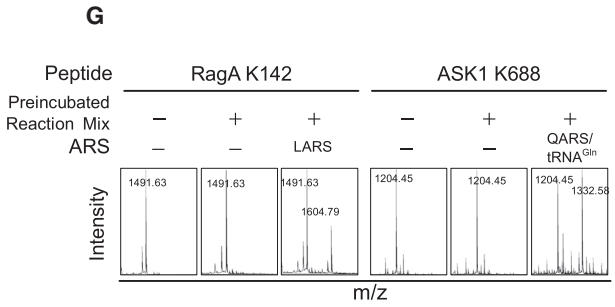

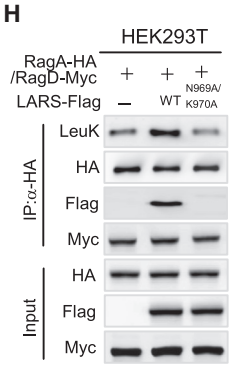

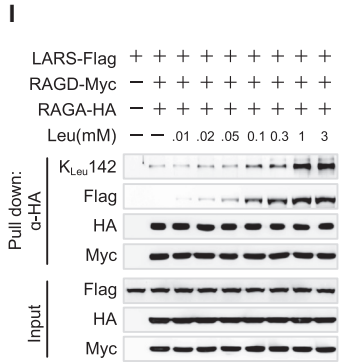

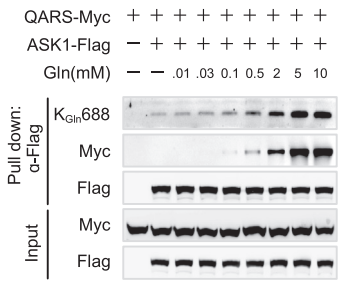

Figure 4. ARSs Selectively Recruit and Efficiently Modify Substrates

(A and B) The kinetic parameters of LARS toward leucine employing intact RagA, toward RagA-K142 (A), and QARS toward glutamine employing intact ASK1, toward ASK1-K688 (B) were determined (n = 3, mean ± SD). The catalytic efficiencies (k_{cat}/K_M, $s^{-1}M^{-1}$) were calculated.

(C and D) Recombinant RagA (C) and ASK1 (D) were subject to leucylation and glutaminylation by LARS and QARS, respectively, *in vitro* (n = 3, mean ± SD). A total of 1 mM leucine was present in the leucylation reactions and 8 mM glutamine was present in the glutaminylation reactions. The sites of modifications and the levels of modifications of each site were determined.

(E and F) RagA (E) and ASK1 (F) were incubated, respectively, with LARS- and QARS-pre-incubated solution alone and with corresponding ARSs added back to the pre-incubated solution. The leucylation on K142 of RagA and the glutaminylation on K688 of ASK1 were detected. RagD was co-expressed with RagA and LARS to facilitate the formation of RagA-LARS-RagD complex. See also Figure S3.

(legend continued on next page)

SIRT3 effectively decreased K142 leucylation in RagA and K688 glutaminylation in ASK1, with an estimated catalytic efficiency (k_{cat}/K_M) to remove K142 leucylation in RagA at 7.76×10^6 (Figures 5C and 5D). Moreover, the LARS-catalyzed RagA K142 leucylation was dose-dependently decreased by SIRT3 (Figure 5E), indicating that the level of RagA K142 leucylation is dynamically regulated by LARS and SIRT3.

To understand the structural basis of how SIRT3 exerts multiple deaminoacylase activities toward K-AAs, we determined the crystal structure of the catalytic domain of SIRT3 (designated SIRT3) in complex with a leucylated peptide (^{638}TRSGK$_{Leu}$VMRRLLR^{649}) derived from human acetyl-CoA synthetase 2 (AceCS2) (Figures 5F and S4). The overall SIRT3 structure is similar to the previously reported structure of SIRT3 in complex with an acetylated AceCS2 peptide (residues 638–649) (PDB: 3GLR) (Jin et al., 2009), with a root-mean-square deviation of 1.49 Å for 253 aligned Cα atoms (Figures S4E–S4G). The SIRT3 structure is composed of a typical Rossmann fold, a well-known NAD^+-binding module, and a small domain containing a four-helical bundle and a zinc-binding motif. The AceCS2-K$_{Leu}$ peptide adopts an extended T-shaped conformation and packs against a shallow groove on the surface of the SIRT3 enzyme (Figure 5G). The interaction between the AceCS2-K$_{Leu}$ peptide and SIRT3 is primarily mediated by main-chain hydrogen bonds formed between residues G641 and V643 of the AceCS2-K$_{Leu}$ peptide and residues G295, Q296, and L298 of SIRT3. Therefore, the primary sequence of the substrate does not appear to be critical for catalysis. Moreover, K$_{Leu}$642 is not specifically recognized, and the hydrophobic pocket is sufficiently large to accommodate groups larger than K$_{Leu}$642 (Figure 5H), which is evident from the crystal structure of SIRT3-AceCS2-K$_{ac}$-ADPR (PDB: 3GLT) (Jin et al., 2009). Notably, similar substrate-binding sites are also found in other known human sirtuin structures, providing possible explanations for the multi-specificity of SIRT1 to K-AAs. Together, the structural analyses supported our observations that SIRT1 and SIRT3 are multi-specific deaminoacylases.

Lending further support that deacetylases could be deaminoacylases, nuclear magnetic resonance (NMR) assays detected the generation of 2′-*O*-leucyl-ADP-ribose (Figure 5I), the generation of NAM, but decrease of NAD^+ (Figure 5J) during the deleucylation of synthetic leucylated K142 peptide by SIRT3 *in vitro*. Moreover, NAM dose-dependently inhibited the deaminoacylase activity of SIRT3 (Figure 5K), while deacetylation-defective SIRT3^{H248A} (Jin et al., 2009) failed to catalyze deleucylation (Figure 5L).

Reversible Leucylation Regulates mTORC1 Activity

We found that either leucine supplementation or LARS overexpression increased the global leucylation levels in HEK293T cells (Figures 6A and 6B). Notably, leucine supplementation to the culture media increased global leucylation (Figure 6C) and K142 of RagA leucylation (Figure 6D) within 15 min. The quick response of leucylation to leucine treatment and the coincident response time between leucylation and mTORC1 activation (Yoshida et al., 2015) suggest that leucylation is a possible underlying mechanism in the activation of mTORC1. This hypothesis is further supported by the overexpression of LARS, but not that of a leucylation-defective LARS$^{F50A/Y52A}$, inducing leucylation and activating mTORC1, as determined by the phosphorylation of S6K (p-S6K) and 4EBP1 (p-4EBP1) (Figure 6E). Moreover, the leucine analog leucinol (Han et al., 2012) inhibited LARS-induced leucylation and decreased LARS-induced mTORC1 activation in HEK293T cells (Figure 6F), and knocking down LARS in HEK293T cells largely abrogated the mTORC1 response to leucine supplementation (Figure 6G). Furthermore, reintroduced wild-type, but not leucylation-defective LARS$^{F50A/Y52A}$, restored mTORC1 response to leucine supplementation in LARS knockdown HEK293T cells (Figure 6H). These results collectively confirmed that LARS senses intracellular leucine and regulates mTORC1 through regulating RagA leucylation.

Given that K142 is the most dynamically leucylated lysine in RagA (Figures 2D and 4C), and the K142 of RagA is close to the GTP-binding region of RagA (Figure S5A) and is reported to be important for mTORC1 regulation (Deng et al., 2015), the molecular mechanism underlying K$_{Leu}$142 of RagA-mediated mTORC1 regulation was studied. The leucylation on K142 was confirmed. The synthetic leucylated RagA peptide produced an MS/MS spectrum identical to that of the liver cancer proteome, and by means of a synthetic unleucylated peptide produced an MS/MS spectrum differing from the above two spectra by a leucine modification (Figure S6A). Moreover, the synthetic leucylated RagA peptide eluted from the high-performance liquid chromatography column at the same time as that of the peptide from the proteome (Figure S6A). Furthermore, since K142 peptide of RagA is equivalent to the K203 peptide of RagB, we further observed that the leucylation levels of both RagA and RagB were elevated by methyl-leucine supplementation, which increases intracellular leucine levels (Zoncu et al., 2011), to the culture media of HEK293T cells (Figure 6I). The GTP loading of Rag A was increased from 33.4% to 78.0% upon leucine supplementation, resembling an effect of substituting K142 to leucine to mimic the effects of constitutive leucylation, which has GTP loading of about 80% and is not responsive to leucine supplementation. Conversely, the substitution of K142 with non-amide bond modifiable and positive charge-retaining arginine decreased their GTP loading to about 35% and abrogated RagA's response to leucine supplementation (Figure 6J). Similar effects were observed for RagB when its K203 was switched to leucine and arginine, respectively (Figure S6B). These results demonstrate that the leucylation on K142 of RagA and K203 of RagB may serve as key leucylation sites to

(G) The leucylation on K142 RagA peptide and the glutaminylation on K688 ASK1 peptide were detected by MS after the peptides were incubated with pre-incubated solution alone and with corresponding ARSs added back to the pre-incubated solution.

(H) RagA/RagD were co-expressed with LARS or LARS$^{N969A/K970A}$. The leucylation levels of affinity-purified RagA were detected.

(I) Overexpressed LARS, RagA, and RagD were purified from HEK293T cells. The LARS-RagA interaction and K142 of RagA leucylation were detected after equal amount of these proteins were incubated *in vitro* in the presence of indicated levels of leucine.

(J) Overexpressed QARS and ASK1 were purified from HEK293T cells. The QARS-ASK1 interaction and K688 of ASK1 glutaminylation were detected after equal amounts of these proteins were incubated *in vitro* in the presence of indicated levels of glutamine.

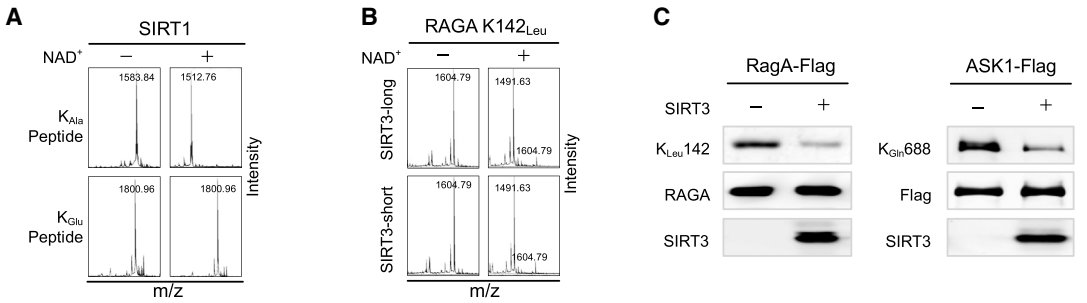

D

Substrate	K_{cat}(s^{-1})	K_m (μM)	K_{cat}/K_m ($s^{-1}M^{-1}$)
K_{Leu}142 of RagA	2.56 ±0.41	0.33 ±0.08	7.76 x 10^6 ±5.31x10^4

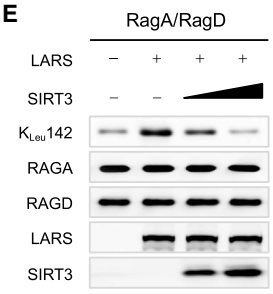

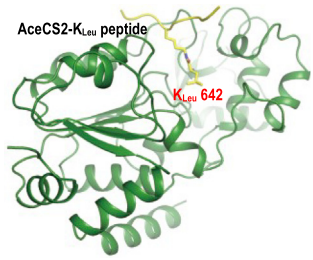

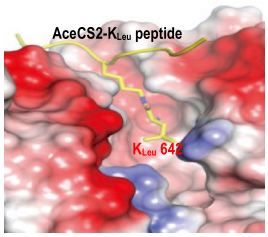

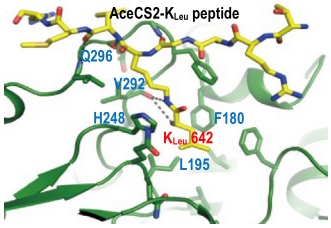

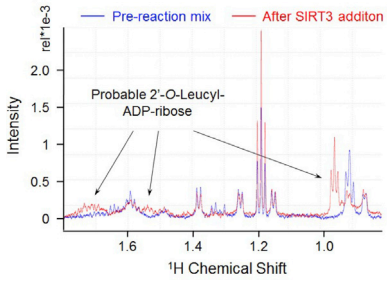

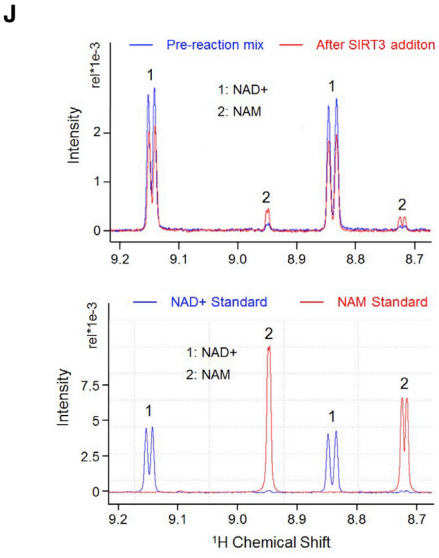

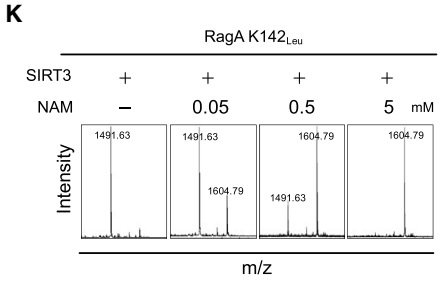

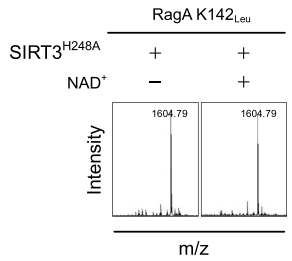

(legend on next page)

activate mTORC1. Seeking further confirmation of this conclusion, we found that RagA^{K142L} had weaker interactions with Ragulator and GATOR1, known GEF and GAP of RagA, respectively (Bar-Peled et al., 2012; Wolfson et al., 2017), whereas RagA^{K142R} had much stronger interactions with Ragulator and GATOR1 (Figure S6C). Moreover, RagA^{K142L} had lower, whereas RagA^{K142R} had higher GTPase activity in the presence of GATOR1 and Ragulator (Figure S6D). These results indicated that leucylation could also alter GTP loading of RagA through altering its interactions with Ragulator and GATOR1 and changing GTPase activity of RagA. We further tested the ability of RagA and RagA^{K142L} and RagA^{K142R}, which bound more tightly and weakly, respectively, than that of RagA with raptor (Figure 6K) in RagA knockdown HEK293T cells, in regulating S6 kinase (S6K) and 4E-binding protein 1 (4-EBP1). While reintroduced RagA elevated the phosphorylation levels of S6K and 4-EBP1 dependent on leucine, reintroduced RagA^{K142L} constitutively elevated the phosphorylation levels of S6K and 4-EBP1 while rendering them less sensitive to methyl-leucine supplementation (Figure 6L); conversely, reintroduced RagA^{K142R} failed to activate mTORC1 and had no effect on restoring mTORC1 responsiveness to methyl-leucine treatment (Figure 6M).

Furthermore, deleucylase *SIRT3* knockdown by *shRNA* increased RagA K_{Leu}142, global leucylation, p-S6K, and p-4EBP1 levels (Figure 6N), whereas the overexpression of SIRT3, but not that of a catalytic dead SIRT3^{H248A}, decreased RagA K_{Leu}142, global leucylation, p-S6K, and p-4EBP1 levels in HEK293T cells (Figure 6O). Moreover, the livers of *Sirt3* knockout *129/C57BL/6* mice (*Sirt3*$^{-/-}$) exhibited higher RagA K_{Leu}142 and S6K and 4EBP1 phosphorylation levels than those found in the wild-type mice (Figure 6P). Furthermore, SIRT3 localized to the lysosome, the site at which mTORC1 activation occurs and LARS is targeted (Zoncu et al., 2011) in a leucine starvation-enhanced manner (Figure 6Q). Lastly, deleucylation active SIRT1 overexpression-decreased p-S6K and p-4EBP1 levels in HEK293T cells were reversed by LARS overexpression (Figure 6R). These results were consistent with documented observations that Sirt3 ablation activates mTOR in mice (Sundaresan et al., 2009) and SIRT1 negatively regulates mTORC1 (Ghosh et al., 2010; Wang et al., 2011), and in line with leucylation being reversed by SIRT1 and SIRT3 (Figure S2F).

Lastly, knockout of *GCN2* in HEK293T cells did not affect the ability LARS overexpression to activate mTORC1 (Figure S6E), excluding the possibility that LARS overexpression-induced mTORC1 activation was due to inactivation of GCN2, a reported upstream inhibitor of mTORTC1 (Ye et al., 2015), through reducing uncharged tRNA^{Leu}.

ASK1 Glutaminylation Inhibits Apoptosis

The K688 of the extracellular apoptotic signal sensor ASK1 is located at the ATP-binding site of ASK1 (Figure S5B) and is glutaminylated (Figure S6A; Table S1), indicating possible roles for glutaminylation in the regulation of apoptosis. QARS interacts with ASK1 (Figure 7A), consistent with ASK1 being a potential glutaminylation substrate of QARS (Figure 4F). Incubation of purified QARS with ASK1 augmented K688 glutaminylation and inactivated its kinase activity, detected by radiometric assays, toward its substrate myelin basic protein (MBP) in a glutamine- and QARS-dependent manner (Figure 7B), showing that kinase activity of ASK1 is under regulation by QARS activity. Moreover, QARS glutamine-dependently inactivates wild-type ASK1, but not a glutaminylation memetic lysine 688 to glutamine switch mutant ASK1 (K688Q) that had diminished kinase activity or a non-glutaminylation memetic lysine 688 to arginine switch mutant ASK1 (K688R) that retained kinase activity (Figure 7C). These results showed that glutaminylation on K688 negatively regulates kinase activity of ASK1, a notion further substantiated by the fact that supplementation of glutamine (Figure 7D) or methyl-glutamine (Figure 7E) decreased the kinase activity of ASK1. K688R showed similar potency while K688Q exhibited a much weaker potency for decreasing the phosphorylation levels of JNK and p38, which serve as apoptotic readouts (Zarubin and Han, 2005), when compared with the wild-type ASK1, when both were overexpressed at similar levels in HeLa cells. Moreover, methyl-glutamine also exerted stronger apoptosis-protective effects in cells overexpressing ASK1 than in cells overexpressing either K688Q or K688R (Figure 7E).

Under glutamine-limiting (1 mM) conditions, the overexpression of QARS, but not that of the glutaminylation-defective

Figure 5. Deacetylases Remove K-AAs

(A) Representative results of SIRT1-catalyzed de-K-AA reactions. The ability of SIRT1 to dealanylate the synthetic TSSK2 (testis-specific serine/threonine-protein kinase 2)-derived K_{Ala}246-containing peptide (upper) and deglutamylate the synthetic CDKL5 (cyclin-dependent kinase-like 5)-derived K_{Glu}825-containing peptide (lower) were determined. See also Figure S2F.

(B) Representative results of SIRT3-catalyzed de-K-AA reactions. The ability of purified long- and short-form SIRT3 to deleucylate the synthetic K_{Leu}142 of RagA peptide was determined *in vitro*.

(C) Purified RagA and ASK1 from NAM-treated HEK293T cells were subject to demodification by SIRT3 *in vitro*. The K_{Leu}142 in RagA and K_{Gln}688 levels in ASK1 were detected in the absence or presence of SIRT3 together with NAD^+.

(D) Deleucylation kinetic parameters of SIRT3 toward K_{Leu}142 of RagA were determined (n = 3, mean ± SD).

(E) The K_{Leu}142 levels of RagA were determined for purified RagA that was incubated with LARS alone or LARS with different levels of SIRT3.

(F) The overall structure of SIRT3 in complex with leucylated lysine peptide (^{638}TRSGK$_{Leu}$VMRRLLR^{649}) derived from human acetyl-CoA synthetase 2. The peptide is colored yellow and K_{Leu} is shown as stick representation. See also Figure S4.

(G) The complex structure revealed that the AceCS2-K_{Leu} peptide adopts an extended T-shaped conformation and packs against a shallow groove on the surface of SIRT3.

(H) Close-up view of the complex structure revealed that the side chain of K_{Leu} inserts into a deep and hydrophobic pocket.

(I) The production of 2′-*O*-leucyl-ADP-ribose (red signals and arrows) in the deleucylation reaction mediated by SIRT3 was monitored by NMR analysis.

(J) The addition of SIRT3 into the deleucylation mix led to a decrease in NAD^+ signals (marked as 1) and increase in NAM signals (marked as 2), as monitored by NMR.

(K) The deleucylation activity of SIRT3 against the synthetic K_{Leu}142 peptide was tested in the presence of various concentrations of NAM.

(L) The deleucylation ability of deacetylation-catalytic dead SIRT3^{H248A} toward the K_{Leu}142 peptide was determined.

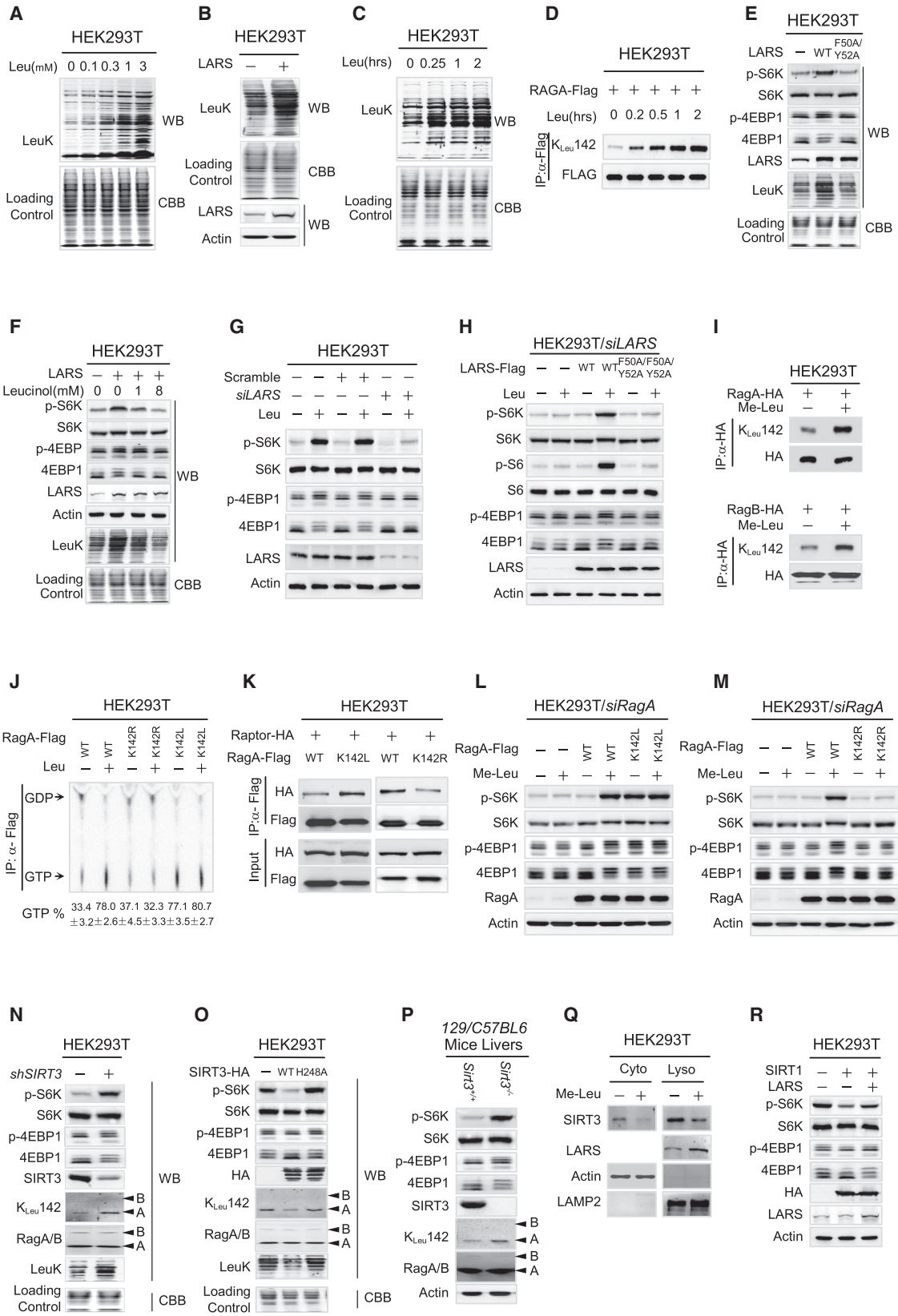

(legend on next page)

QARS^{K496A}, increased endogenous K688 glutaminylation but inhibited apoptosis induced by FAS antibody in HeLa cells (Figure 7F). Conversely, QARS knockdown partially abrogated the ability of glutamine to increase K688 glutaminylation and suppress apoptosis induced by FAS antibody in HeLa cells (Figure 7G). These results suggest that glutamine suppresses apoptosis, at least partly, through QARS-mediated glutaminylation. Supporting this notion, overexpression of SIRT3, which deglutaminylates K688 of ASK1 (Figure 5C), partially abrogated the ability of glutamine to suppress apoptosis in HeLa cells (Figure 7H). Conversely, ablation of deglutaminylase *Sirt3* in mouse hepatocytes decreased their apoptosis rate and made them more resistant to further cell death induced by FAS antibody (Figure 7I). Taken together, these results are in line with previous reports that SIRT3 acts as a pro-apoptotic factor (Allison and Milner, 2007; Kim et al., 2010), and confirms that glutamine- and QARS-promoted glutaminylation is responsible, at least partly, for the anti-apoptotic effects of glutamine and QARS.

DISCUSSION

In addition to their canonical tRNA charging activity, we provided evidence from *in vitro* biochemical and cellular biological assays to show that ARSs have additional aminoacyl transferase activities, which are capable of sensing sufficiency of specific amino acids and transmitting amino acid signals to regulate cellular physiologies. The sporadically reported aminoacyl transferase activities of prokaryotic ARSs, such as lysyl-tRNA synthetase of *Escherichia coli* and methionyl-tRNA synthetase of *Bacillus stearothermophilus* (Gilreath et al., 2011; Hountondji et al., 2000; Yanagisawa et al., 2010), are part of non-canonical activities of ARSs from bacteria to human. The chemical basis of aminoacyl transferase activities of ARSs is that ARSs produce aminoacyl-AMP, which contains a reactive bond that is capable of modifying ε-amine of lysine in proteins (Moellering and Cravatt, 2013; Weinert et al., 2013). Formation of K-AAs by ARSs enables proteins without amino acid-binding sites to be regulated by amino acids, providing additional avenues to understand different amino acids convey distinct signals to cells. These findings provided a whole new formal basis for addressing previous confounding observations such as the tRNA synthetases having potential roles in the nucleus, given that protein synthesis ostensibly occurs in the cytoplasm (Guo and Schimmel, 2013).

Two requirements need to be met to form K-AAs in proteins: a given ARS picks up its cognate amino acid and this ARS interacts with its substrates. While ARSs are designed in nature to specifically bind their respective cognate amino acids, the binding of ARSs to their substrate proteins, at least for LARS and QARS we studied, is dependent on amino acid levels. This resolved the potential competition between activities of tRNA charging and aminoacylation of ARS. It only requires subphysiologic levels of amino acids to saturate tRNA charging activity of ARSs to ensure that cells have their essential protein synthesis function. The formation of K-AAs, however, only happens when levels of amino acids reach around their physiological levels. Therefore, K-AAs can specifically sense sufficiency of amino acids and transduce the signal of amino acids. It is worth noting that *in vitro* assays revealed that some ARSs, such as YARS, have weaker ability to form K-AAs than their ability to form charged tRNAs. The K_M and k_{cat} for YARS-catalyzed *in vitro* tyrosylation reaction on a synthetic topoisomerase (DNA) IIβ (TOP2B)-derived peptide were 0.2887 μM and 0.0102 s^{-1}, respectively (Figure S6F). Although the K_M of tyrosine is similar for YARS to form tyrosylation and for tRNA^{Tyr} charging (0.3 μM), the k_{cat} for tyrosylation reaction is significantly lower than that of tRNA^{Tyr} charging reaction, which was reported as 1.49 s^{-1} (Jia et al., 2003). This difference reminds us that transmitting amino acid signals through K-AAs may differ in efficiency among amino acids and substrates.

Figure 6. Leucylation of RagA and/or RagB Activates mTORC1

(A) The global leucylation levels of HEK293T cells cultured in leucine-free RPMI 1640 supplemented with various levels of leucine were detected by western blotting (WB). Protein levels in each sample were normalized by Coomassie brilliant blue (CBB) staining (hereafter for global modification detection).

(B) The global leucylation levels of LARS-overexpressing HEK293T cells were compared with those of HEK293T cells.

(C and D) Time-dependent leucylation levels of global proteins (C) and K142 of RagA (D) were determined.

(E and F) The global leucylation levels, and p-S6K and p-4EBP1 levels of HEK293T cells were compared with those of LARS (wild-type [WT])- and LARS$^{F50A/Y52A}$-overexpressing HEK293T cells (E), and LARS-overexpressing HEK293T cells cultured in DMEM supplemented with the indicated level of leucinol (F).

(G) The responses of p-S6K and p-4EBP1 levels to leucine HEK293T cells and LARS knockdown HEK293T cells were compared.

(H) The responses of p-S6K, p-4EBP1, and p-S6 levels to leucine supplementation were compared among *LARS* knockdown HEK293T, *LARS* knockdown HEK293T-expressing LARS, and HEK293T-expressing LARS$^{F50A/Y52A}$.

(I) The K142 leucylation levels of RagA and K203 leucylation levels of RagB were detected in RagA and RagB overexpressed from HEK293T cells cultured with and without methyl-leucine supplementation of the culture media. K_{Leu}142 antibody was employed for detecting K_{Leu}203, as the leucylated lysines of these two proteins are flanked by the same amino acids.

(J) HEK293T cells transfected with RagA protein and its mutants were labeled with 50 μCi/mL orthophosphate for 8 hr. The bound GTP and GDP in RagA, RagA^{K142L}, and RagA^{K142R} from either non-treated or leucine-treated HEK293T cells were eluted and analyzed by polyethyleneimine cellulose thin-layer chromatography. See also Figure S6B.

(K) The binding of RagA, RagA K142L, and RagA K142R to Raptor was compared when Raptor was co-expressed with each of them in HEK293T cells.

(L and M) The responses of p-S6K and p-4EBP1 levels to methyl-leucine supplementation were compared in HEK293T cells expressing similar levels of either wild-type RagA or RagA^{K142L} (L), and in HEK293T cells expressing similar levels of either wild-type RagA or RagA^{K142R} (M).

(N and O) The K_{Leu}142, p-S6K, and p-4EBP1 levels were compared between HEK293T and *SIRT3* knockdown HEK293T cells (N), and among HEK293T cells and HEK293T cells expressing either SIRT3 or inactive SIRT3^{H248A} (O).

(P) The K_{Leu}142, p-S6K, and p-4EBP1 levels of the livers of *Sirt3* knockout *129/C57BL/6* mice and their isogenic wild-type mice were detected.

(Q) HEK293T cells were lysed and the lysosomal fraction (Lyso) was isolated. Lysosome-associated membrane protein 2 (LAMP2) was used as a lysosome marker. The amounts of SIRT3 and LARS were detected in lysosome fractions with and without methyl-leucine supplementation of the culture media. Levels of SIRT3 in the cytosol were detected as control.

(R) The p-S6K and p-4EBP1 levels in HEK293T cells, SIRT1-overexpressing HEK293T cells, and SIRT1- and LARS-overexpressing HEK293T cells were detected.

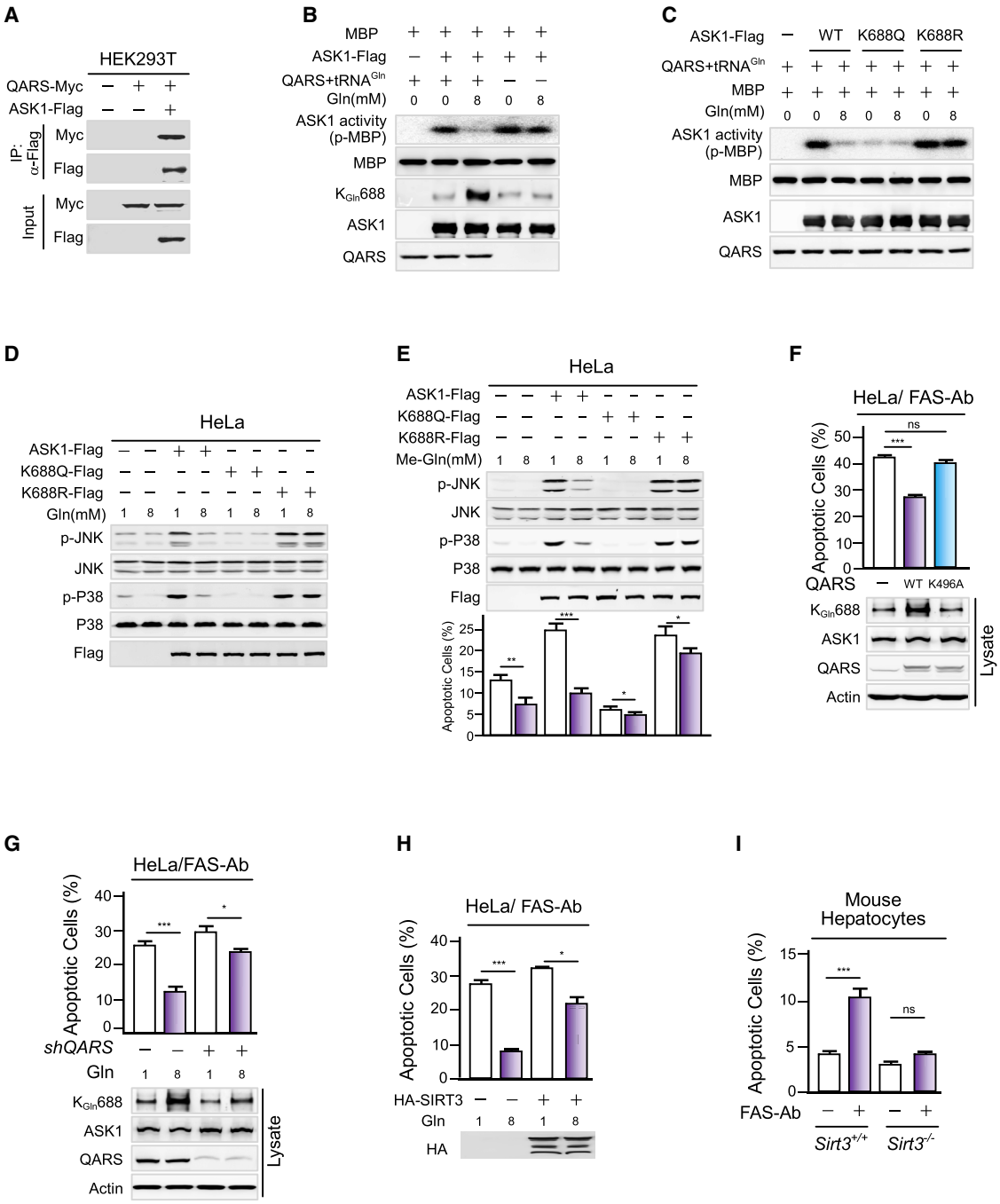

Figure 7. Glutaminylation Suppresses Apoptosis by Inactivating ASK1

(A) Myc-tagged QARS was co-overexpressed with ASK1-FLAG in HEK293T cells. Interaction between QARS and ASK1 was assayed by co-immunoprecipitation (IP).

(B and C) *In vitro* glutamine- and $tRNA^{Gln}$-dependent ASK1 kinase activities toward MBP and the *in vitro* glutaminylation of ASK1 K688 were assayed when purified ASK1 was incubated in the presence or absence of QARS and $tRNA^{Gln}$ (B), and when purified ASK1 was incubated with wild-type, K688Q, and K688R ASK1, respectively (C).

(D and E) The P-JNK and P-P38 levels of HeLa cells and ASK1-, $ASK1^{K688Q}$-, and $ASK1^{K688R}$-overexpressing HeLa cells were determined at low (1 mM) and high (8 mM) concentrations of glutamine (D) or at low (1 mM) and high (8 mM) concentrations of methyl-glutamine supplementation (E). The apoptosis rates were measured for methyl-glutamine supplementation. Representative western blot and apoptosis rates (n = 3, means ± SD) are shown.

(F) The effects of overexpression of QARS or $QARS^{K496A}$ on the endogenous K688 glutaminylation and apoptosis rate were examined in FAS antibody-treated HeLa cells, respectively (n = 3, means ± SD).

(G) The effects of glutamine on the endogenous K688 glutaminylation and apoptosis rates of HeLa cells and QARS knockdown HeLa cells were detected following FAS treatment (n = 3, means ± SD).

(legend continued on next page)

The significance of requirement for interactions between ARSs and their substrates for amino acid signal transduction is echoed by the finding that eukaryotic ARSs acquired interacting domains during evolution that endowed them with functional diversity (Jia et al., 2008; Rho et al., 1999) and ARSs mutation-associated diseases are often due to mutations in interacting domains (Kim et al., 2011). Moreover, amino acids such as leucine and arginine are sensed by ARSs and by other machinery functioning in different pathways (Chantranupong et al., 2016; Wolfson et al., 2016), reflecting the fact that a given amino acid can exert its regulations through different sensors.

The involvement of sirtuins, such as SIRT1 and SIRT3, in deaminoacylation processes not only makes K-AAs reversibly regulated, but also connects K-AAs to energy metabolism in cells because SIRT levels are regulated by cellular nutrient status (Hirschey et al., 2011) and the activities of sirtuins are dependent on the levels of NAD^+, an energy status indicator. Moreover, sirtuins are involved in removal of multiple metabolite-derived lysine PTMs (Du et al., 2011). These facts suggest that while the traditional view is that phosphate, ubiquitin, and other molecules are the major modifications, it is becoming increasingly clear that metabolite-derived modifications also should merit concern. Many metabolites, including all amino acids, modify the ε-amines of lysines, indicating that lysine residues in proteins function as "antennae" for metabolic signaling processes. It is worth noting that in cells, one metabolite can be sensed by multiple sensors. We previously found that metabolites such as ketoglutarate are sensed by multiple proteins such as PHD2 (prolyl hydroxylase domain-containing protein 2), TET (ten-eleven translocation), and histone demethylases (Xu et al., 2011; Zhao et al., 2009). LARS and previously identified Sestrin2 both sense leucine and regulate mTORC1. This ensures that signals of a metabolite/amino acid can be precisely sensed for different pathways, since different sensors have distinct affinities to the metabolite/amino acid and subcellular localizations. In summary, the addition of amino acids into the growing body of lysine modifiers not only expanded the functions of ARSs and deacetylases, but also may expand our knowledge of the enormous regulatory space encompassed by all of the protein targets modified by the total set of 20 standard amino acids.

STAR★METHODS

Detailed methods are provided in the online version of this paper and include the following:

- KEY RESOURCES TABLE
- CONTACT FOR REAGENT AND RESOURCE SHARING
- EXPERIMENTAL MODEL AND SUBJECT DETAILS
  - Cell Lines
  - Mouse Lines
  - Clinical Samples
- METHOD DETAILS
  - Preparation of Free Metabolites-Free Proteome
  - CobB Treatment to Release Lysine Modifiers
  - Detection of Metabolites
  - NMR Analysis
  - Proteomic Analysis
  - Protein Digestion
  - Liquid Chromatography-Mass Spectrometry
  - Data Processing, Validation and Analysis
  - Peptides Quantitation and Kinetic Analysis
  - Preparation of ARSs and ARS2s
  - *In Vitro* Aminoacylation
  - *In Vitro* De-aminoacylation
  - X-Ray Structural Study
  - *In Vivo* RagA/B GTPase Assay
  - In Vitro GTPase Assay
  - ASK1 Kinase Assay
  - Preparation of Antibodies
  - Apoptosis Assay
- QUANTIFICATION AND STATISTICAL ANALYSIS
- DATA AND SOFTWARE AVAILABILITY

SUPPLEMENTAL INFORMATION

Supplemental Information includes six figures and three tables and can be found with this article online at https://doi.org/10.1016/j.cmet.2017.10.015.

AUTHOR CONTRIBUTIONS

S.-M.Z. conceived the project. S.-M.Z., W.X., and Y.X. supervised experiments, analyzed the data, and wrote the manuscript. X.-D.H., C.-F.Y., J.N., J.-N.Z., G.-Q.Y., P.-Y.Y., Y.W., Y.-Z.M., Y.L., J.-Y.Z., X.-H.W., F.-S.G., P.-C.L., and F.L. carried out the proteomic survey and metabolomics survey, *in vitro* aminoacylation and deaminoacylation, and molecular biological analysis. X.-D.H., W.-C.S., and E.-D.W. made ARSs. Y.X., W.G., and J.L. carried out crystal structural analysis. X.-D.H., Y.-P.A., and H.-R.T. performed the NMR analysis. All of the authors discussed the results and commented on the manuscript.

ACKNOWLEDGMENTS

We thank Dr. Sunghoon Kim of National Seoul University for providing pCMV-SPORT6 LARS. We thank staff members of beamline BL17U and BL19U at SSRF for assistance in data collection. This work was supported by grants from the State Key Development Programs (973) of Basic Research of China (nos. 2013CB911204, 2013CB531200, 2013CB945100, and 2015AA020913), the Ministry of Science and Technology of China (2016YFA0500700), the National Natural Science Foundation of China (nos. 31330023, 81722021, 81471454, 31671453, 81771627, 31521003, U1432242, and 31425008), 863 programs of China (2015AA020913), and Science and Technology Municipal Commission of Shanghai, China (16JC1405300).

Received: June 6, 2017
Revised: August 17, 2017
Accepted: October 26, 2017
Published: November 30, 2017

(H) The apoptosis rates of HeLa cells and SIRT3-overexpressing HeLa cells were tested when cells were cultured in media containing 1 mM and 8 mM of glutamine, respectively (n = 3, means ± SD).
(I) The pro-apoptotic abilities of FAS antibody were tested in the hepatocytes of *129/C57BL6* and Sirt3$^{-/-}$ *129/C57BL/6* mice, respectively (n = 3, means ± SD). Statistical significance is defined as not significant (ns), *p < 0.05, **p < 0.01, and ***p < 0.001.

REFERENCES

Adams, P.D., Afonine, P.V., Bunkoczi, G., Chen, V.B., Davis, I.W., Echols, N., Headd, J.J., Hung, L.W., Kapral, G.J., Grosse-Kunstleve, R.W., et al. (2010). PHENIX: a comprehensive Python-based system for macromolecular structure solution. Acta Crystallogr. D Biol. Crystallogr. *66*, 213–221.

Airas, R.K., and Cramer, F. (1986). Pyrophosphate-caused inhibition of the aminoacylation of tRNA by the leucyl-tRNA synthetase from *Neurospora crassa*. Eur. J. Biochem. *160*, 291–296.

Allison, S.J., and Milner, J. (2007). SIRT3 is pro-apoptotic and participates in distinct basal apoptotic pathways. Cell Cycle *6*, 2669–2677.

Balakin, K.V., Ivanenkov, Y.A., Kiselyov, A.S., and Tkachenko, S.E. (2007). Histone deacetylase inhibitors in cancer therapy: latest developments, trends and medicinal chemistry perspective. Anticancer Agents Med. Chem. *7*, 576–592.

Bar-Peled, L., Schweitzer, L.D., Zoncu, R., and Sabatini, D.M. (2012). Ragulator is a GEF for the rag GTPases that signal amino acid levels tomTORC1. Cell *150*, 1196–1208.

Berlanga, J.J., Santoyo, J., and de Haro, C. (1999). Characterization of a mammalian homolog of the GCN2 eukaryotic initiation factor 2 alpha kinase. Eur. J. Biochem. *265*, 754–762.

Blander, G., and Guarente, L. (2004). The Sir2 family of protein deacetylases. Annu. Rev. Biochem. *73*, 417–435.

Blomstrand, E., Eliasson, J., Karlsson, H.K., and Kohnke, R. (2006). Branched-chain amino acids activate key enzymes in protein synthesis after physical exercise. J. Nutr. *136*, 269S–273S.

Chantranupong, L., Scaria, S.M., Saxton, R.A., Gygi, M.P., Shen, K., Wyant, G.A., Wang, T., Harper, J.W., Gygi, S.P., and Sabatini, D.M. (2016). The CASTOR proteins are arginine sensors for the mTORC1 pathway. Cell *165*, 153–164.

Chantranupong, L., Wolfson, R.L., and Sabatini, D.M. (2015). Nutrient-sensing mechanisms across evolution. Cell *161*, 67–83.

Chen, Y., Sprung, R., Tang, Y., Ball, H., Sangras, B., Kim, S.C., Falck, J.R., Peng, J., Gu, W., and Zhao, Y. (2007). Lysine propionylation and butyrylation are novel post-translational modifications in histones. Mol. Cell Proteomics *6*, 812–819.

Colak, G., Xie, Z.Y., Zhu, A.Y., Dai, L.Z., Lu, Z.K., Zhang, Y., Wan, X.L., Chen, Y., Cha, Y.H., Lin, H.N., et al. (2013). Identification of lysine succinylation substrates and the succinylation regulatory enzyme CobB in *Escherichia coli*. Mol. Cell Proteomics *12*, 3509–3520.

Deng, L., Jiang, C., Chen, L., Jin, J.L., Wei, J., Zhao, L.L., Chen, M.H., Pan, W.J., Xu, Y., Chu, H.S., et al. (2015). The ubiquitination of RagA GTPase by RNF152 negatively regulates mTORC1 activation. Mol. Cell *58*, 804–818.

Dong, J.S., Qiu, H.F., Garcia-Barrio, M., Anderson, J., and Hinnebusch, A.G. (2000). Uncharged tRNA activates GCN2 by displacing the protein kinase moiety from a bipartite tRNA-Binding domain. Mol. Cell *6*, 269–279.

Du, J., Zhou, Y., Su, X., Yu, J.J., Khan, S., Jiang, H., Kim, J., Woo, J., Kim, J.H., Choi, B.H., et al. (2011). Sirt5 is a NAD-dependent protein lysine demalonylase and desuccinylase. Science *334*, 806–809.

Efeyan, A., Comb, W.C., and Sabatini, D.M. (2015). Nutrient-sensing mechanisms and pathways. Nature *517*, 302–310.

Emsley, P., Lohkamp, B., Scott, W.G., and Cowtan, K. (2010). Features and development of Coot. Acta Crystallogr. D Biol. Crystallogr. *66*, 486–501.

Faergeman, N.J., Wadum, M., Feddersen, S., Burton, M., Kragelund, B.B., and Knudsen, J. (2007). Acyl-CoA binding proteins; structural and functional conservation over 2000 MYA. Mol. Cell Biochem. *299*, 55–65.

Ghosh, H.S., McBurney, M., and Robbins, P.D. (2010). SIRT1 negatively regulates the mammalian target of rapamycin. PLoS One *5*, e9199.

Gilreath, M.S., Roy, H., Bullwinkle, T.J., Katz, A., Navarre, W.W., and Ibba, M. (2011). beta-Lysine discrimination by lysyl-tRNA synthetase. FEBS Lett. *585*, 3284–3288.

Guo, M., and Schimmel, P. (2013). Essential nontranslational functions of tRNA synthetases. Nat. Chem. Biol. *9*, 145–153.

Han, J.M., Jeong, S.J., Park, M.C., Kim, G., Kwon, N.H., Kim, H.K., Ha, S.H., Ryu, S.H., and Kim, S. (2012). Leucyl-tRNA synthetase is an intracellular leucine sensor for the mTORC1-signaling pathway. Cell *149*, 410–424.

Hattori, K., Naguro, I., Runchel, C., and Ichijo, H. (2009). The roles of ASK family proteins in stress responses and diseases. Cell Commun. Signal. *7*, 9.

Hirschey, M.D., Shimazu, T., Huang, J.Y., Schwer, B., and Verdin, E. (2011). SIRT3 regulates mitochondrial protein acetylation and intermediary metabolism. Cold Spring Harb. Symp. Quant. Biol. *76*, 267–277.

Holden, M.T.G., Feil, E.J., Lindsay, J.A., Peacock, S.J., Day, N.P.J., Enright, M.C., Foster, T.J., Moore, C.E., Hurst, L., Atkin, R., et al. (2004). Complete genomes of two clinical *Staphylococcus aureus* strains: evidence for the rapid evolution of virulence and drug resistance. Proc. Natl. Acad. Sci. USA *101*, 9786–9791.

Hountondji, C., Beauvallet, C., Pernollet, J.C., and Blanquet, S. (2000). Enzyme-induced covalent modification of methionyl-tRNA synthetase from *Bacillus stearothermophilus* by methionyl-adenylate: identification of the labeled amino acid residues by matrix-assisted laser desorption-ionization mass spectrometry. J. Protein Chem. *19*, 563–568.

Jia, J., Arif, A., Ray, P.S., and Fox, P.L. (2008). WHEP domains direct noncanonical function of glutamyl-prolyl tRNA synthetase in translational control of gene expression. Mol. Cell *29*, 679–690.

Jia, J., Li, B., Jin, Y., and Wang, D. (2003). Expression, purification, and characterization of human tyrosyl-tRNA synthetase. Protein Expr. Purif. *27*, 104–108.

Jin, L., Wei, W., Jiang, Y., Peng, H., Cai, J., Mao, C., Dai, H., Choy, W., Bemis, J.E., Jirousek, M.R., et al. (2009). Crystal structures of human SIRT3 displaying substrate-induced conformational changes. J. Biol. Chem. *284*, 24394–24405.

Kato, Y. (2014). The formation of lipid hydroperoxide-derived amide-type lysine adducts on proteins: a review of current knowledge. In Lipid Hydroperoxide-Derived Modification of Biomolecules, Y. Kato, ed. (Springer), pp. 21–39.

Kern, D., and Lapointe, J. (1981). The catalytic mechanism of glutamyl-tRNA synthetase of *Escherichia coli*. A steady-state kinetic investigation. Eur. J. Biochem. *115*, 29–38.

Kim, H.S., Patel, K., Muldoon-Jacobs, K., Bisht, K.S., Aykin-Burns, N., Pennington, J.D., van der Meer, R., Nguyen, P., Savage, J., Owens, K.M., et al. (2010). SIRT3 is a mitochondria-localized tumor suppressor required for maintenance of mitochondrial integrity and metabolism during stress. Cancer Cell *17*, 41–52.

Kim, S., You, S., and Hwang, D. (2011). Aminoacyl-tRNA synthetases and tumorigenesis: more than housekeeping. Nat. Rev. Cancer *11*, 708–718.

Ko, Y.G., Kim, E.Y., Kim, T., Park, H., Park, H.S., Choi, E.J., and Kim, S. (2001). Glutamine-dependent antiapoptotic interaction of human glutaminyl-tRNA synthetase with apoptosis signal-regulating kinase 1. J. Biol. Chem. *276*, 6030–6036.

Kodera, H., Osaka, H., Iai, M., Aida, N., Yamashita, A., Tsurusaki, Y., Nakashima, M., Miyake, N., Saitsu, H., and Matsumoto, N. (2015). Mutations in the glutaminyl-tRNA synthetase gene cause early-onset epileptic encephalopathy. J. Hum. Genet. *60*, 97–101.

Laskowski, R.A., MacArthur, M.W., Moss, D.S., and Thornton, J.M. (1993). PROCHECK: a program to check the stereochemical quality of protein structures. J. Appl. Cryst. *26*, 283–291.

Law, I.K., Liu, L., Xu, A., Lam, K.S., Vanhoutte, P.M., Che, C.M., Leung, P.T., and Wang, Y. (2009). Identification and characterization of proteins interacting with SIRT1 and SIRT3: implications in the anti-aging and metabolic effects of sirtuins. Proteomics *9*, 2444–2456.

Lebedev, A.A., Young, P., Isupov, M.N., Moroz, O.V., Vagin, A.A., and Murshudov, G.N. (2012). JLigand: a graphical tool for the CCP4 template-restraint library. Acta Crystallogr. D Biol. Crystallogr. *68*, 431–440.

Lombard, D.B., Alt, F.W., Cheng, H.L., Bunkenborg, J., Streeper, R.S., Mostoslavsky, R., Kim, J., Yancopoulos, G., Valenzuela, D., Murphy, A., et al. (2007). Mammalian Sir2 homolog SIRT3 regulates global mitochondrial lysine acetylation. Mol. Cell. Biol. *27*, 8807–8814.

McCoy, A.J. (2007). Solving structures of protein complexes by molecular replacement with Phaser. Acta Crystallogr. D Biol. Crystallogr. *63*, 32–41.

Minor, W., Cymborowski, M., Otwinowski, Z., and Chruszcz, M. (2006). HKL-3000: the integration of data reduction and structure solution—from diffraction images to an initial model in minutes. Acta Crystallogr. D Biol. Crystallogr. *62*, 859–866.

Moellering, R.E., and Cravatt, B.F. (2013). Functional lysine modification by an intrinsically reactive primary glycolytic metabolite. Science *341*, 549–553.

Nazario, M., and Evans, J.A. (1974). Physical and kinetic studies of arginyl transfer ribonucleic acid ligase of *Neurospora*. A sequential ordered mechanism. J. Biol. Chem. *249*, 4934–4936.

Ravel, J.M., Wang, S.F., Heinemeyer, C., and Shive, W. (1965). Glutamyl and glutaminyl ribonucleic acid synthetases of *Escherichia coli* W. Separation, properties, and stimulation of adenosine triphosphate-pyrophosphate exchange by acceptor ribonucleic acid. J. Biol. Chem. *240*, 432–438.

Rebsamen, M., Pochini, L., Stasyk, T., de Araujo, M.E., Galluccio, M., Kandasamy, R.K., Snijder, B., Fauster, A., Rudashevskaya, E.L., Bruckner, M., et al. (2015). SLC38A9 is a component of the lysosomal amino acid sensing machinery that controls mTORC1. Nature *519*, 477–481.

Rho, S.B., Kim, M.J., Lee, J.S., Seol, W.G., Motegi, H., Kim, S., and Shiba, K. (1999). Genetic dissection of protein-protein interactions in multi-tRNA synthetase complex. Proc. Natl. Acad. Sci. USA *96*, 4488–4493.

Saitoh, M., Nishitoh, H., Fujii, M., Takeda, K., Tobiume, K., Sawada, Y., Kawabata, M., Miyazono, K., and Ichijo, H. (1998). Mammalian thioredoxin is a direct inhibitor of apoptosis signal-regulating kinase (ASK) 1. EMBO J. *17*, 2596–2606.

Schrodinger LLC (2010). The PyMOL Molecular Graphics System, Version 1.3r1 (Schrodinger).

Schulze, W.X., and Usadel, B. (2010). Quantitation in mass-spectrometry-based proteomics. Annu. Rev. Plant Biol. *61*, 491–516.

Sundaresan, N.R., Gupta, M., Kim, G., Rajamohan, S.B., Isbatan, A., and Gupta, M.P. (2009). Sirt3 blocks the cardiac hypertrophic response by augmenting Foxo3a-dependent antioxidant defense mechanisms in mice. J. Clin. Invest. *119*, 2758–2771.

Taylor, P.M. (2014). Role of amino acid transporters in amino acid sensing. Am. J. Clin. Nutr. *99*, 223s–230s.

Thorens, B., and Mueckler, M. (2010). Glucose transporters in the 21st century. Am. J. Physiol. Endocrinol. Metab. *298*, E141–E145.

Wang, R.H., Kim, H.S., Xiao, C., Xu, X., Gavrilova, O., and Deng, C.X. (2011). Hepatic Sirt1 deficiency in mice impairs mTorc2/Akt signaling and results in hyperglycemia, oxidative damage, and insulin resistance. J. Clin. Invest. *121*, 4477–4490.

Wang, S., Tsun, Z.Y., Wolfson, R.L., Shen, K., Wyant, G.A., Plovanich, M.E., Yuan, E.D., Jones, T.D., Chantranupong, L., Comb, W., et al. (2015). Metabolism. Lysosomal amino acid transporter SLC38A9 signals arginine sufficiency to mTORC1. Science *347*, 188–194.

Weinert, B.T., Iesmantavicius, V., Wagner, S.A., Scholz, C., Gummesson, B., Beli, P., Nystrom, T., and Choudhary, C. (2013). Acetyl-phosphate is a critical determinant of lysine acetylation in *E. coli*. Mol. Cell *51*, 265–272.

Winn, M.D., Ballard, C.C., Cowtan, K.D., Dodson, E.J., Emsley, P., Evans, P.R., Keegan, R.M., Krissinel, E.B., Leslie, A.G., McCoy, A., et al. (2011). Overview of the CCP4 suite and current developments. Acta Crystallogr. D Biol. Crystallogr. *67*, 235–242.

Wolfson, R.L., Chantranupong, L., Saxton, R.A., Shen, K., Scaria, S.M., Cantor, J.R., and Sabatini, D.M. (2016). Sestrin2 is a leucine sensor for the mTORC1 pathway. Science *351*, 43–48.

Wolfson, R.L., Chantranupong, L., Wyant, G.A., Gu, X., Orozco, J.M., Shen, K., Condon, K.J., Petri, S., Kedir, J., Scaria, S.M., et al. (2017). KICSTOR recruits GATOR1 to the lysosome and is necessary for nutrients to regulate mTORC1. Nature *543*, 438–442.

Xu, W., Yang, H., Liu, Y., Yang, Y., Wang, P., Kim, S.H., Ito, S., Yang, C., Wang, P., Xiao, M.T., et al. (2011). Oncometabolite 2-hydroxyglutarate is a competitive inhibitor of alpha-ketoglutarate-dependent dioxygenases. Cancer Cell *19*, 17–30.

Yanagisawa, T., Sumida, T., Ishii, R., Takemoto, C., and Yokoyama, S. (2010). A paralog of lysyl-tRNA synthetase aminoacylates a conserved lysine residue in translation elongation factor P. Nat. Struct. Mol. Biol. *17*, 1136–1143.

Ye, J., Palm, W., Peng, M., King, B., Lindsten, T., Li, M.O., Koumenis, C., and Thompson, C.B. (2015). GCN2 sustains mTORC1 suppression upon amino acid deprivation by inducing Sestrin2. Genes Dev. *29*, 2331–2336.

Yoon, M.S., Son, K., Arauz, E., Han, J.M., Kim, S., and Chen, J. (2016). Leucyl-tRNA synthetase activates Vps34 in amino acid-sensing mTORC1 signaling. Cell Rep. *16*, 1510–1517.

Yoshida, S., Pacitto, R., Yao, Y., Inoki, K., and Swanson, J.A. (2015). Growth factor signaling to mTORC1 by amino acid-laden macropinosomes. J. Cell Biol. *211*, 159–172.

Zarubin, T., and Han, J.H. (2005). Activation and signaling of the p38 MAP kinase pathway. Cell Res. *15*, 11–18.

Zhang, Z., Tan, M., Xie, Z., Dai, L., Chen, Y., and Zhao, Y. (2011). Identification of lysine succinylation as a new post-translational modification. Nat. Chem. Biol. *7*, 58–63.

Zhao, S., Lin, Y., Xu, W., Jiang, W., Zha, Z., Wang, P., Yu, W., Li, Z., Gong, L., Peng, Y., et al. (2009). Glioma-derived mutations in IDH1 dominantly inhibit IDH1 catalytic activity and induce HIF-1alpha. Science *324*, 261–265.

Zoncu, R., Bar-Peled, L., Efeyan, A., Wang, S.Y., Sancak, Y., and Sabatini, D.M. (2011). mTORC1 senses lysosomal amino acids through an inside-out mechanism that requires the vacuolar H+-ATPase. Science *334*, 678–683.

STAR★METHODS

KEY RESOURCES TABLE

REAGENT or RESOURCE	SOURCE	IDENTIFIER
Antibodies		
RagA	Cell Signaling Technology	Cat#4357S; RRID: AB_10545136
RagD	Cell Signaling Technology	Cat#4470S; RRID: AB_1950380
RagC	Cell Signaling Technology	Cat#5466S; RRID: AB_10692651
SIRT3	Cell Signaling Technology	Cat#5490S; RRID: AB_10828246
GCN2	Cell Signaling Technology	Cat#3302S; RRID: AB_10694800
phospho-T389,S6K	Cell Signaling Technology	Cat#9234S; RRID: AB_2269803
S6K	Cell Signaling Technology	Cat#9202S; RRID: AB_331676
phospho-T37/46 4EBP1	Cell Signaling Technology	Cat#2855S; RRID: AB_560835
4EBP1	Cell Signaling Technology	Cat#9452S; RRID: AB_331692
phospho-S240/244 S6	Cell Signaling Technology	Cat#5364S; RRID: AB_10694233
S6	Cell Signaling Technology	Cat#2217S; RRID: AB_331355
LAMP2	Cell Signaling Technology	Cat#49067S
phospho-T183/Y185 JNK	Cell Signaling Technology	Cat#4668S; RRID: AB_823588
JNK	Cell Signaling Technology	Cat#9252S; RRID: AB_2250373
phospho-T180/Y182 P38	Cell Signaling Technology	Cat#9211S; RRID: AB_331641
P38	Cell Signaling Technology	Cat#9212S; RRID: AB_330713
ASK1	Cell Signaling Technology	Cat#8662S; RRID: AB_11220434
MBP	Cell Signaling Technology	Cat#78896S
p18	Cell Signaling Technology	Cat#8975S; RRID: AB_10860252
DEPDC5	Omnimabs	Cat#OM276949
NPRL2	Santa Cruz	Cat#Sc-376986
Flag	Abmart	Cat#M20008; RRID: AB_2713960
HA	Abmart	Cat#M20003
Myc	Abmart	Cat#M20002
LARS	Abcam	Cat#ab31534; RRID: AB_776011
QARS	Abcam	Cat#ab103675; RRID: AB_10862316
FAS	Merck Millipore	Cat#05-201; RRID: AB_309653
Actin	GenScript	Cat#A00702-100
anti-mouse secondary antibodies	GenScript	Cat#A00160; RRID: AB_1968937
anti-rabbit secondary antibodies	GenScript	Cat#A00098; RRID: AB_1968815
pan-leucyllyisne (LeuK) antibody	This Study	N/A
K142Leu RagA	This Study	N/A
K688Gln ASK1	This Study	N/A
Chemicals, Peptides, and Recombinant Proteins		
Penicillin-Streptomycin	Invitrogen	Cat#15070063
Leucine-free RPMI 1640	USBiological Life Science	Cat#R8999-03
DMEM, no glutamine	Gibco	Cat#11960044
methoxyamine hydrochloride	Sigma	Cat#226904
N-methyl-N-(tert-butyldimethylsilyl) trifluoroacetamide	Sigma	Cat#394882
sequencing grade modified trypsin	Promega	Cat#V5111
TFA	Sigma	Cat#302031
synthetic aminoacylated peptides	GL Biochem	N/A
protein-A Sepharose bead	Merck Millipore	Cat#16-156
EDC	Thermo	Cat#77149

(*Continued on next page*)

Continued

REAGENT or RESOURCE	SOURCE	IDENTIFIER
NHS	Thermo	Cat#24500
NAM	Sigma	Cat#72340
Critical Commercial Assays		
^{32}P-phosphate, 5mCi, Disodium Phosphate in 1mL Water	PerkinElmer	Cat#NEX011
[gamma-^{32}P] ATP	PerkinElmer	Cat#BLU002
FITC Annexin V Apoptosis Detection Kit I	BD Pharmingen	Cat#556547
Deposited Data		
Atomic coordinate of the SIRT3-Leu-AceCS2 complex	This Study	PDB: 5YTK
Raw data	This Study	https://doi.org/10.17632/g9njsrf5wr.1
Experimental Models: Cell Lines		
Human: HeLa	ATCC	ATCC Number:CCL-2
HEK293T	ATCC	ATCC Number:CRL-11268
Oligonucleotides		
36 siRNA Oligonucleotides	This Study	Table S2
Recombinant DNA		
37 Recombinant DNAs	This Study	Table S3
Software and Algorithms		
Prism 5	GraphPad	www.graphpad.com
PyMOL	Schrodinger	http://www.pymol.org/
ImageQuant TL	GE	http://imagequanttl.updatestar.com/
MaxQuant	Matthias Mann	http://www.coxdocs.org/doku.php?id=maxquant:start

CONTACT FOR REAGENT AND RESOURCE SHARING

Further information and requests for reagents may be directed to and will be fulfilled by the Lead Contact, Shi-Min Zhao (zhaosm@fudan.edu.cn).

EXPERIMENTAL MODEL AND SUBJECT DETAILS

Cell Lines

HEK293T (human embryonic kidney cell lines, female) and HeLa (human cervix cancer cell lines, female) cells were cultured in either normal Dulbecco's Modified Eagle's Medium (DMEM) (HyClone) supplemented with 10% newborn bovine serum (NCS) (Biochrom.), 100 units/ml penicillin (Invitrogen) and 100μg/ml streptomycin (Invitrogen) or conditioned medium made from DMEM base (Sigma-Aldrich) as specified. Cell transfection was performed using PEI or calcium phosphate methods. Deacetylase inhibitor treatments were carried out by adding NAM (5mM, final concentration) to the culture medium 5 hours before harvesting. Leucine starvation in mTOR activity detection was achieved by resining cells with leucine-free RPMI 1640 (USBIOLOGICOL LIFE SCIENCE) twice before incubating cells in leucine-free RPMI 1640 for 60 min, followed by stimulation with 1mM leucine for 5–60 min. The low glutamine was achieved by culturing cells in DMEM with 1 mM glutamine (Gibco) for 1 hour and the high glutamine was achieved by culturing cells in DMEM with 8 mM glutamine (Gibco) for 1 hour. Primary hepatocytes were isolated from starved 8-week-old adult male C57BL/129 mice (25-30g). The cells were plated in M199 medium supplemented with 100U/ml penicillin, 100μg/ml streptomycin, 10% foetal bovine serum, 500nM dexamethasone (dex; Sangon Biotech), 10nM insulin (Actrapid, Novo Nordisk), at a density of 2.5×10^5 cells/well on 6-well plates or 1×10^5 cells/24-well plates.

Mouse Lines

All animal procedures were in accordance with the animal care committee at Fudan University. The global germ-line *Sirt3* knockout (*Sirt3*-KO) mice (C57BL/129 background) were generated as previous described and their genotyping were confirmed by PCR (Lombard et al., 2007). Briefly, *Sirt3*-KO mice were generated by employing Cre-LoxP recombination technology. A 5.8-kb genomic DNA fragment containing exon 1-3 was inserted flanking the pGK-Neo cassette of the pGEM7 vector. A 3-kb genomic DNA fragment containing exon4 was inserted on the opposite side of the pGK-Neo cassette. The Sirt3-KO mice genotyping were confirmed by PCR with primers: 5'-CTTCTGCGGCTCTATACACAG-3', 5'-TGCAACAAGGCTTTATCTTCC-3' and 5'-TACTGAATATCAGTGG GAACG-3'.

Clinical Samples

Three human liver cancer tissues (sample #1: male, 63 years old, left lobe, BCLC stage B; sample #2: male, 52 years old, right lobe, BCLC stage A1; sample #3: female, 53 years old, right lobe, BCLC stage A2) were obtained from Shanghai Cancer Center, Fudan University with the signed consent from the patients and approval of the ethics committee of Fudan University.

METHOD DETAILS

Preparation of Free Metabolites-Free Proteome

Human liver cancer tissues were homogenized before lysed in pre-chilled PBS buffer (NaCl 1.37 mM, KCl 27 mM, Na_2HPO_4 100 mM, KH2PO4 18 mM, pH7.4). Homogenized or cultured cells were lysed by sonication (20,000-40,000 Hz) in PBS buffer. The debris of samples was removed by centrifugation (x 1,000g) and the proteins in the supernatant were precipitated with 85% (final concentration) by adding pre-chilled acetone. The proteome were obtained by centrifugation (x 1,000g) and the noncovalent bound metabolites were removed by repeatedly (3x) resuspension and centrifugation (x 1,000g) cold 85% acetone. The prepared free metabolites-free proteome were dried in air before they were subject to further manipulation.

CobB Treatment to Release Lysine Modifiers

The proteome of either human liver cancer tissue or fractions of HEK293T cells was incubated with recombinant CobB that was over-expressed and purified from *E. Coli* BL21 (DE3) pLysS at protein:protein ratio of 100:1 in a 600 μl reaction solution contained 50 mM HEPES (pH 7.5), 6 mM $MgCl_2$, 1 mM DTT, 1 mM NAD^+ and 1 mM PMSF. The reaction was allowed to continue at 37°C for 4 hours before it is stopped by 4x volume ice-cold methanol. The released modifiers were analyzed by GC-MS and the metabolites were identified by comparing MS/MS spectra against NIST chemical database employing Angilent Enhanced Chem Station.

Detection of Metabolites

Metabolites were oximated by methoxyamine hydrochloride (239 mM) in pyridine at 70°C for 60-90min, followed by derivatization at 30°C for 30-60 minutes with 20 μl N-methyl-N-(tert-butyldimethylsilyl) trifluoroacetamide dissolved in 80 μl pyridine. Filtrated sample (2 μl) was resolved with Agilent 19091S-433HP-5MS (29.8 m x 250 μm x 0.25 μm) and analyzed by Agilent 6890-5973 GC-MS system. The retention time and area of GC were used to detect and quantitate metabolites in combination with MS/MS spectra.

NMR Analysis

All the one-dimensional 1H NMR spectra were acquired at 298 K on a Bruker Advance III 600 MHz NMR spectrometer (600.13 MHz for proton frequency) equipped with an inverse cryogenic probe (Bruker Biospin, Germany) using the first increment of the gradient selected NOESY pulse sequence (NOESYGPPR1D: recyle delay-G1-900-T1-900-tm-G2-900-acquisition). 64 transients were collected into 32 k data points with a spectral width of 20 ppm for each sample.

Proteomic Analysis

Proteomic analysis was carried out as following: proteome of liver cancer were digested with sequencing grade modified trypsin (Promega) overnight at the protease/protein ratio in 1:50. The resulted peptide mixture was acidified with TFA to pH $\sqrt{3}$ and resolved by nano-LC and analyzed by on-line electrospray tandem mass spectrometry. Raw MS files were analyzed by MaxQuant version 1.4.1.2. MS/MS spectra were searched by the Andromeda search engine against the SwissProt-human database (Released 2014-04-10).

Protein Digestion

Protein concentration in the crude protein extract was estimated by Bradford reagent (Bio-Rad). About 10 mg of protein extract was dissolved and denatured in 6 M urea and 2 M thiourea, reduced with 1 mM DTT for 45 min. at room temperature, and carbamidomethylated with 5 mM iodoacetamide for 45 min. at room temperature in the dark. Alkylated proteins were digested first with endopeptidase Lys-C (Waco) for 3 h, after which the solution was diluted four times with deionized water, and then further digested with sequencing grade modified trypsin (Promega) overnight. The protease/protein ratio was in both cases 1:50. The resulting peptide mixture was acidified with TFA to pH =3.

Liquid Chromatography-Mass Spectrometry

The peptides were suspended with 25μl solvent A (A: water with 0.1% formic acid; B: ACN with 0.1% formic acid), separated by nano-LC and analyzed by on-line electrospray tandem mass spectrometry. The experiments were performed on a nano

Acquity UPLC system (Waters Corporation, Milford, USA) connected to a LTQ Orbitrap XL (for liver proteome analysis) or Q Exactive hybrid quadrupole-Orbitrap mass spectrometer (for $K142_{Leu}$ of RagA and $K688_{Gln}$ of ASK1 peptides analysis) (Thermo Fisher Scientific, San Jose, CA, USA) equipped with an online nano-electrospray ion source. Each sample was loaded onto the Thermo Scientific Acclaim PepMap C18 column (100 μm x 2cm, 3 μm particle size), with a flow of 10 μl/min for 3 min and subsequently separated on the analytical column (Acclaim PepMap C18, 75 μm x 15cm) with a linear gradient, from 5% B to 45% B in 75 min. The column was re-equilibrated at initial conditions for 15 min. The column flow rate was maintained at 300nL/min and column temperature was maintained at 40°C. The electrospray voltage of 1.8 kV versus the inlet of the mass spectrometer was used.

LTQ Orbitrap XL mass spectrometer was operated in the data-dependent mode to switch automatically between MS and MS/MS acquisition. Survey full-scan MS spectra with one microscan (m/z 400-1800) was acquired in the Obitrap with a mass resolution of 60,000 at m/z 400, followed by MS/MS of the eight most-intense peptide ions in the LTQ analyzer. The automatic gain control (AGC) was set to 1000,000 ions, with maximum accumulation times of 500 ms. The minimum MS signal for triggering MS/MS was set to 500 and single charge state was rejected. Dynamic exclusion was used with two microscans and 90 s exclusion duration. For MS/MS, precursor ions were activated using 35% normalized collision energy at the default activation q of 0.25 and an activation time of 30 ms. For MS/MS, we used an isolation window of 3 m/z and automatic gain control (AGC) was set to 20 000 ions, with maximum accumulation times of 120 ms. Q Exactive mass spectrometer was operated in the data-dependent mode to switch automatically between MS and MS/MS acquisition. Survey full-scan MS spectra (m/z 350-1600) were acquired with a mass resolution of 70K, followed by ten sequential high energy collisional dissociation (HCD) MS/MS scans with a resolution of 17.5K. In all cases, one microscan was recorded using dynamic exclusion of 30 seconds. MS/MS fixed first mass was set at 100.

Data Processing, Validation and Analysis

Raw MS files were analyzed by MaxQuant version 1.4.1.2. MS/MS spectra were searched by the Andromeda search engine against the SwissProt-human database (Release 2014-04-10) containing forward and reverse sequences (total of 40492 entries including forward and reverse sequences). Additionally, the database included 248 common contaminants. In the main Andromeda search precursor mass and fragment mass had an initial mass tolerance of 5 ppm and 0.05 Da for Q Exactive, 5ppm and 0.5 Da for LTQ Orbitrap XL, respectively. The search included variable modifications of methionine oxidation. Minimal peptide length was set to seven amino acids and a maximum of four miscleavages was allowed. The false discovery rate (FDR) was set to 0.01 for peptide and protein identifications, all scores of peptides were above 40. In the case of identified peptides that are all shared between two proteins, these are combined and reported as one protein group.

Peptides Quantitation and Kinetic Analysis

Quantitation of peptides or aminoacylated peptides for stoichiometric analysis and kinetic assays was achieved by digesting proteins into tryptic peptides, following by peptide counting or measuring the ratio of areas of LC peaks corresponding to modified and unmodified peptides that matches m/z values of these peptides.

The Orbitrap Fusion mass spectrometer was used to analyze tryptic peptides generated from the target proteins. The LC-MS was operated in the data-dependent mode to switch automatically between MS and MS/MS acquisition. Survey full-scan MS spectra (m/z 350-1600) were acquired in Orbitrap with a mass resolution of 60, 000 at m/z 200. The AGC taget was set to 300, 000, and the maximum injection time was 50ms. MS/MS acquisition was performed in Orbitrap with 3 s cycle time, the resolution was 15, 000 at m/z 200. The intensity threshold was 50,000, and the maximum injection time was 200 ms. The AGC target was set to 200,000, and the isolation window was 2 m/z. Ions with charge states 2+, 3+, and 4+ were sequentially fragmented by higher energy collisional dissociation (HCD) with a normalized collision energy (NCE) of 30%, fixed first mass was set at 120. In all cases, one micro scan was recorded using dynamic exclusion of 30 seconds. The overexpressed proteins from HEK293T cells and treated HEK293T cells were affinity purified and digested with trypsin. The aminoacylated tryptic peptides were analyzed by MS/MS sequencing.

For quantification of targeted aminoacylated peptides, a published method (Schulze and Usadel, 2010) was employed. Briefly, a ratio of aminoacylated peptide signal (the total ion counts (TIC) of aminoacylated form) to the total peptide signal (TIC of aminoacylated form + TIC of non-aminoacylated form) were calculated according to the following equation: *TICK-AA*/(*TICK-AA*+*TICnon-K-AA*) = *Ratio of K-AA* (*RK-AA*).

The kinetic parameters of LARS, QARS and YRAS toward their substrates were determined by measuring the formation of aminoacylations in intact proteins or peptides, respectively. K_{cat}s and K_ms of leucine, glutamine and tyrosine were obtained by varying amino acids levels when their protein or peptide substrates were fixed at indicated levels. K_{cat}s and K_ms of proteins and peptides were obtained by varying protein or peptide levels when their corresponding amino acids levels were fixed at indicated levels. The quantitation of K_{Leu}142 in RagA was achieved by measuring peptide abundance that corresponding to DLIFK$_{Leu}$ER and DLIFK. The quantitation of K_{Gln}688 in ASK1 was achieved by measuring peptide abundance that corresponding to VVLGK$_{Gln}$GTYGIVYAGR and GTYGIVYAGR. The K_{cat}s and K_ms of LARS and QARS toward peptides were determined by measuring the velocities of producing modified peptides. To determine K_{cat}s and K_ms of SIRT3 toward RagA, *in vitro* leucylated RagA was employed as substrate. The velocities of DLIFK$_{Leu}$ER decreasing were determined. Purified recombinant SIRT3 (0.05 μM final Concentration) was incubated in a 300 μl reaction mix contained 50 mM HEPES (pH 7.5), 1 mM DTT 6 mM $MgCl_2$ and 1.0 mM NAD+. The reactions were stopped with 100 mM HCl and 160 mM acetic acid during linear phases of reactions. All K_{cat}s and K_ms were deduced from Michaelis-Menten equation.

Preparation of ARSs and ARS2s

All ARSs and ARS2s were cloned into pcDNA3.1b-C-Flag with a tag at C-terminus of the ARSs and ARS2s genes. Each ARSs or ARS2s was expressed in HEK293T cells and affinity purified by commercial available Flag-tagged beads. The Flag-peptide eluted ARSs or ARS2s were used for *in vitro* aminoacylation and other analysis.

In Vitro Aminoacylation

In vitro aminoacylation reactions were carried out in a 30μl reaction mix contains 50 mM HEPES (pH 7.5), 25 mM KCl, 2 mM $MgCl_2$,5 mM amino acid, 4 mM ATP, 10 nM ARS,0.05 mg/ml synthetic substrate peptide. The final pH of the each reaction mix was adjusted to 7.5 before adding ARSs or ARS2s. The reaction was allowed continue for 3 hours at 37°C. The peptide was desalted by passing through a C18 ZipTip (Millipore) and subject to analyzation by a MALDI-TOF/TOF mass spectrometer (SCIEX-5800).

In Vitro De-aminoacylation

In vitro de-aminoacrylation reactions were carried out in a 30 μl reaction mix contains 50 mM HEPES (pH 7.5), 6 mM $MgCl_2$, 1 mM DTT, 1 mM NAD^+, 0.05 mg/ml synthetic aminoacylated peptide,1 mg/ml SIRT1, SIRT3 or CobB and 1 mM PMSF. The reaction was allowed continue for 4 hours at 37°C. The peptide was desalted by passing through a C18 ZipTip (Millipore) and subject to analyzation by a MALDI-TOF/TOF mass spectrometer (SCIEX-5800).

X-Ray Structural Study

Purified SIRT3 were mixed with AceCS2-K_{Leu} in 1:5 stoichiometry before crystallization and reached a final concentration of 10mg/mL. The native data were collected at SSRF (Shanghai Synchrotron Radiation Facility in China) beamline BL19U. Data were indexed, integrated and scaled using program HKL3000.

The ORF of human SIRT3 (118-399) was sub-cloned into derived pET vector, which places expression under the control of the T7 promoter. The plasmid was transformed into E.coli BL21 (DE3) for protein expression. The transformant was grown at 37°C to an OD600 of 0.8, and then induced by adding 0.1 mM isopropyl-b-D-thiogalactopyranoside and cultured for 16 h at 15°C. The cells were harvested and lysed. The supernatant was applied onto Ni-NTA columns followed by on-column digestion using Ulp1 enzyme at 4°C for 5hr. Protein was further purified by an anion exchange and a gel filtration chromatography. The protein was concentrated to ~30mg/mL for the biochemical analyses and crystallization. A Leucine-modified lysine (designated AceCS2-K_{Leu}) peptide (^{638}TRSGK$_{Leu}$VMRRLLR^{649}) derived from human Acetyl-CoA Synthetase 2 was synthsized. The K_{Leu} represents residue lysine-leucine 642, in which side-chain amino nitrogen forms an isopeptide bond with the main-chain carboxylic carbon of a Leucine moiety. Purified SIRT3 were mixed with AceCS2-K_{Leu} in 1:5 stoichiometry before crystallization and reached a final concentration of 10mg/mL. The crystals of SIRT3-AceCS2-K_{Leu} were obtained using the hanging-drop, vapour-diffusion method by mixing 1μL complex solution with 1μL reservoir solution containing 0.1 M MES monohydrate (pH 6.2) and 8% PEG 20,000 at 18°C. The native data were collected at SSRF (Shanghai Synchrotron Radiation Facility in China) beamline BL19U. Data were indexed, integrated and scaled using program HKL3000 (Minor et al., 2006). Phase were determined by molecular replacement implemented via program PHASER (McCoy, 2007) in CCP4 package (Winn et al., 2011), using the published structure of SIRT3 in complex with AceCS2-K_{Ac} peptide (PDB: 3GLR) (Jin et al., 2009) as a search model. The model was further manually built with COOT (Emsley et al., 2010) and refined using PHENIX (Adams et al., 2010). The AceCS2-K_{Leu} peptide was built with J Ligand (Lebedev et al., 2012) and merged with SIRT3 structure using COOT. The quality of final model was checked with the PROCHECK program (Laskowski et al., 1993). All structure figures were generated using PyMOL (Schrodinger LLC, 2010).

In Vivo RagA/B GTPase Assay

A reported method was adopted (Han et al., 2012). Briefly, HEK293T cells were washed with phosphate-free DMEM and incubated with 1 ml of phosphate-free DMEM for 1 hour, followed by incubating with 50 μCi of 32P-phosphate/ml for 8 hours. The labeled cells were lysed with pre-chilled lysis buffer (0.5% NP-40, 50 mM Tris [pH 7.5], 100 mM NaCl, 10 mM $MgCl_2$, 1 mM dithiothreitol [DTT], 1 mM phenylmethylsulfonyl fluoride) for 30 minutes on ice. The lysates were then centrifuged at 12,000 g for 15 minutes at 4°C. The supernatant (160 μl) was transferred to a fresh tube, and 16 μl of NaCl (500 mM) was added to inhibit GAP activity. Flag-RagA/B was then immunoprecipitated with anti-Flag antibody and protein-A Sepharose bead for 1 hour at 4°C. The beads were washed with wash buffer 1 (50 mM Tris [pH 8.0], 500 mM NaCl, 5 mM $MgCl_2$, 1 mM DTT, 0.5% Triton X-100) three times at 4°C and then washed with wash buffer 2 (50 mM Tris [pH 8.0], 100 mM NaCl, 5 mM $MgCl_2$, 1 mM DTT, 0.1% Triton X-100) three times at 4 °C. The Flag-RagA/B-bound nucleotides were eluted with 20 ml of elution buffer (2 mM EDTA, 0.2% sodium dodecyl sulfate, 1 mM GDP, 1 mM GTP) at 68 °C for 10 minutes. The eluted nucleotides were applied onto polyethyleneimine cellulose plates (SIGMA) and developed in 0.75 M KH_2PO_4 [pH 3.4] solution. GTP and GDP were visualized and quantified by a phosphoimager (Typhoon FLA 9500, GE).

In Vitro GTPase Assay

In vitro GTPase assay were carried out in a 200μl reaction mix contains 25mM Tris-HCl (Ph 7.5), 5 mM $MgCl_2$, 5 mM KCl, 125 mM NaCl, 1 mM GTP and 0.1% bovine serum albumin with a GTPase assay kit (Innova Biosciences, 602-0120) following the mannufacture's guidance.

ASK1 Kinase Assay

Immunoprecipitated ASK1 was washed three times with wash buffer (50 mM Tris-HCl [pH 7.5], 150 mM NaCl, 5 mM EGTA, 2 mM dithiothreitol, 1 mM phenylmethylsulfonyl fluoride, 1% Triton X-100) and two times with a reaction buffer (20 mM Tris-HCl [pH7.5], 20 mM $MgCl_2$). The reaction was carried out in the reaction buffer in the presence of 0.5 μCi of [γ-^{32}P] ATP for 10 min at 30 °C using

myelin basic protein (MBP) (40 mg/ml) (Sigma) as an exogenous substrate (Saitoh et al., 1998). The samples were resolved by SDS-polyacrylamide gel electrophoresis and the phosphorylated MBP was quantified by a phosphoimager (Typhoon FLA 9500, GE).

Preparation of Antibodies

The pan-leucyllyisne (LeuK) antibody was prepared by using chemically aminoacylated BSA as antigen employing the reported chemical modification approach (Moellering and Cravatt, 2013). Briefly, the lysine leucylation reactions were carried out at room temperature in a 2 ml reaction mix (MES base, pH 7.5) that contains 3.4mg/ml leucine, 35 mg/ml EDC (Thermo) and 40 mg/ ml NHS (Thermo). BSA solution was added to a final concentration of 1 mg/ml. The resulted leucylated BSA was confirmed for modification before subjecting to immunize rabbits. For $K142_{Leu}$ and $K688_{Gln}$ site-specific antibodies, synthetic aminoacylated peptides corresponding to K142 of RagA and K688 of ASK1 were conjugated to OVA as antigen before subjecting to immunize rabbits. All antibodies were made in AbMart Shanghai.

Apoptosis Assay

FITC Annexin V Apoptosis Detection Kit I (BD Pharmingen) was used following the manufacture's guidance. HeLa cells were washed twice with cold PBS and then were suspended in 1X Binding Buffer at a concentration of 1 x 10^6 cells/ml. Transfer 100 μl of the solution (1 x 10^5 cells) to a 5 ml culture tube. Add 5 μl of FITC Annexin V and 5 μl PI. Gently vortex the cells and incubate for 15 min at RT (25°C) in the dark. After adding 400 μl of 1X Binding Buffer to each tube, apoptosis was analyzed by flow cytometry (BD, C6) within 1 hour.

QUANTIFICATION AND STATISTICAL ANALYSIS

Unless specified, results are expressed as means ± SD. Comparisons between groups were made by unpaired 2-tailed Student's t test. Differences were considered statistically significant if P was less than 0.05.

DATA AND SOFTWARE AVAILABILITY

The atomic coordinate of the SIRT3-Leu-AceCS2 complex has been deposited in the Protein Data Bank under PDB: 5YTK. Raw data have been deposited to Mendeley Data and are available at https://doi.org/10.17632/g9njsrf5wr.1.